




Article

Evaluation of Satellite-Derived Signatures for Three Verified Hailstorms in Central Argentina

Anthony C. Bernal Ayala ^{1,*}, Angela K. Rowe ¹, Lucia E. Arena ^{2,3} and Ankur R. Desai ¹¹ Atmospheric and Oceanic Program, College of Letters and Science, University of Wisconsin, Madison, WI 53706, USA; akrowe@wisc.edu (A.K.R.); desai@aos.wisc.edu (A.R.D.)² Laboratorio de Física de la Atmosfera Laura Levi, Facultad de Matemáticas, Astronomía, Física y Computación, Universidad Nacional de Córdoba, Córdoba 5016, Argentina; lucia.arena@unc.edu.ar³ Observatorio Hidrometeorológico de Córdoba, Córdoba 5016, Argentina

* Correspondence: crespo3@wisc.edu

Abstract: Córdoba Province in Argentina is a global hotspot for deep hail-producing storms. Previous studies of hail formation and detection largely relied on satellite snapshots or modeling studies, but lacked hail validation, relying instead on proxy metrics. To address this limitation, this study used hail collected in the mountainous Córdoba region in collaboration with the citizen science program “Cosecheros de Granizo 2018–2020” including from a record-breaking hail event and from the 2018–2019 RELAMPAGO field campaign. Three cases including a MCS and two supercells, which have verified hail in different environment locations relative to the Sierras de Córdoba, were analyzed for multi-spectral signatures in GOES-16 satellite data. Brightness temperatures decreased over time after convective initiation, reaching values cooler than the tropopause with variations around those values of different magnitudes. Overall, all cases exhibited a slight weakening of the updraft and strong presence of smaller ice crystal sizes just prior to the hail report, especially for the larger hailstones. The results demonstrate promise in using satellite proxies for hail detection in multiple environments for different storm modes. The long-term goal is to better understand hail-producing storms and unique challenges of forecasting hail in this region.

Keywords: hail; supercell; mesoscale convective system; geostationary satellite



Citation: Bernal Ayala, A.C.; Rowe, A.K.; Arena, L.E.; Desai, A.R. Evaluation of Satellite-Derived Signatures for Three Verified Hailstorms in Central Argentina. *Meteorology* **2022**, *1*, 183–210. <https://doi.org/10.3390/meteorology1020013>

Academic Editors: Edoardo Bucchignani and Paul D. Williams

Received: 29 March 2022

Accepted: 28 April 2022

Published: 13 May 2022

Publisher's Note: MDPI stays neutral with regard to jurisdictional claims in published maps and institutional affiliations.



Copyright: © 2022 by the authors. Licensee MDPI, Basel, Switzerland. This article is an open access article distributed under the terms and conditions of the Creative Commons Attribution (CC BY) license (<https://creativecommons.org/licenses/by/4.0/>).

1. Introduction

Falling hailstones are some of the most destructive natural phenomena in convectively active regions of the world. In the U.S. alone, damage from hailstorms has exceeded one billion dollars since 1949 [1–4]. Córdoba Province in Argentina, where some of the most intense storms in the world occur [5], experiences frequent hail (e.g., [6,7]) that has destructive impacts on property and agriculture. A challenge in forecasting hail comes from an incomplete understanding of the main environmental and storm internal controls on hail occurrence and size (e.g., [8–10]). While studies have revealed relationships between hail growth and updraft strength, many of these relationships are inferred from observations in the U.S. and Europe (e.g., [11]). Furthermore, proxy soundings used in these studies are unable to represent the variations in microphysical processes that exist within different storm modes (e.g., [12,13]).

There is a need to study hail-producing storms from a global perspective that covers varying environmental conditions and storm modes. This task, however, is limited by a lack of ground-based observations including verified hail reports. Where operational radar data are available, accurate estimations of hail sizes from these observations remain a challenge. Satellite-based proxies for hail have provided global inferences of hail occurrence [7,14–16], but often do not coincide with the ground validation of hail reports. The 2018–2019 Remote sensing of Electrification, Lightning, and Mesoscale/microscale Processes with

Adaptive Ground Observations (RELAMPAGO; [17]) field campaign provided ground-based datasets and ground validation of hail in Argentina and a unique opportunity to improve the understanding of these hail-producing convective systems. Furthermore, the Argentine citizen science campaign “Cosecheros de granizos” (Hail Harvesters) [18], which began in 2018, allowed access to temporal-spatial information of confirmed hail reports and georeferenced data from the RMA1 operational radar in Córdoba, Argentina.

Previous studies agree that most hail events in Southeast South America (SESA) occur during austral summers (DJF), coinciding with large precipitation systems with deep convective cores, especially in northeastern Argentina [15,19,20]. In the U.S., most large hail reports are associated with supercellular convection, while non-supercellular convection storm modes are associated with smaller-diameter hailstones (e.g., [13]). However, multiple limitations have previously made it difficult to study convective modes and severe weather in Argentina such as the lack of high spatial and temporal radar data, surface and upper-air observations, and standardized severe weather reporting. Using operational radar data from 2015 to 2017, Mulholland et al. (2018) [19] found that two-thirds of convective storms near Córdoba, Argentina were characterized as multicellular storms, with convection initiation occurring most frequently between 14:00 and 19:00 UTC (1100–1600 LST) and 23:00 and 06:00 UTC (2000–0300 LST). More specifically for hail-producing storms in this region, Bruick et al. (2019) [15], using a 16-year TRMM dataset and ERA-Interim reanalysis data, also observed a peak in inferred hail activity during the afternoon as well as an overnight peak associated with multicellular systems.

Reanalysis data have revealed that compared with U.S. environments supportive of mesoscale convective systems (MCSs) and discrete supercells, storm environments in central Argentina tend to have larger Convective Available Potential Energy (CAPE) values and weaker low-level vertical wind shear with a rapid transition to MCSs [19]. The South American Low-Level Jet (SALLJ) strongly influences the development of deep multicellular convection over the SESA region by ushering in warm and moist air from the north [15,19–24]. A modeling study in this region [23] showed how moisture fluxes controlled by the strength of the SALLJ, dry air subsidence from the westerlies traversing the Andes Mountains, and lee cyclogenesis are all associated with convective systems developing over the Sierras de Córdoba (SDCs), a mesoscale mountain range in central Argentina. Environments favorable for hailstorms in this region have similarly been characterized by strong upper- and lower-level jets, anomalously warm and moist low levels, and enhanced instability [15].

The previously mentioned studies provided valuable insight into environments favorable for deep convection and hailstorms in this region, but with limitations. In particular, the Bruick et al. (2019) [15] polar-orbiting satellite-based study was limited to a statistical analysis over many years with no hail verification. Geostationary satellite visible and infrared measurements can be exploited to obtain a more comprehensive mapping of hail occurrence with storm lifecycle [25–28]. Brightness temperatures are directly associated with the intensity of convection (e.g., [29,30]). Müller et al. (2018) [31] showed how a strong vertical updraft could be inferred from the cooling rate, defined by the temporal change of the brightness temperatures of the cells between two subsequent satellite images. To have hail in a convective cloud requires a strong vertical updraft that can support the weight of a large hailstone, and therefore brightness temperatures can be used to infer whether a convective system could support hail. Geostationary satellite data including infrared channels and lightning flash counts from GOES-16 were used by Borque et al. (2020) [32] to look at the spatio-temporal co-evolution of storm kinematics (updraft area and lifespan), cloud-top cooling rates, and lightning production for a severe storm that occurred on 11 December 2018 in east-central Córdoba Province in Argentina. This study only focused on a single supercellular system relating GOES-16 data to severe weather. Ribeiro et al. (2019) [25] highlighted the use of data from the GOES-16 mesoscale domain sector, a ground-based C-band radar, and a ground-based lightning network to investi-

gate multiple satellite-derived trends for detecting thunderstorm intensification relative to validated hail fall from a supercell in southeastern Brazil.

Here, this project seeks to demonstrate how GOES-16 satellite-derived parameters can be used to monitor deep convection and how specific satellite signatures may be associated with hail production. In particular, satellite-based inferences of hail were investigated for convective storms in mountainous central Argentina using verified hail reports for different storm modes. This work builds off previous case studies in SESA to uniquely include a case of verified hail from a MCS near Córdoba and compare it to verified hail events from supercells in this region. Studies that focus on South America, or Argentina more specifically, have been historically limited because there are not many continuous ground-based observations, there is a limitation in coverage of ground-based radar data in the mountainous Córdoba region, and there is limited hail validation that can be related to convective mode, temporal evolution, and environmental conditions. This gap is approached through a satellite-focused analysis of verified hail-producing storms in the Córdoba region including a record-breaking hail event [33,34] and from a MCS during RELAMPAGO [17], allowing us to relate hail occurrence to remotely sensed inferences of hail for various storm modes.

The objectives are to (1) identify the storm mode of these hail-producing storms; (2) describe the environmental conditions under which they form; and (3) determine the temporal and spatial evolution of these storms from satellite data to relate to where and when the hail was observed. Section 2 describes the datasets and methods used to address these objectives. Section 3 describes the cases analyzed including their storm mode, evolution, associated environmental conditions, and temporal evolution of satellite data to the hail reports, and Section 4 provides a discussion of the results in the context of previous work and the implications of those results.

2. Data and Methods

2.1. Hail Events

Verified hail reports were available using hail samples collected through a Ministry of Science and Technology of the Córdoba Province program, “Cosecheros de Granizo” [18] for samples collected in 2018 and the Hydro-Meteorological Observatory of Córdoba for samples collected in 2020. Hail was collected in various localities around the SDCs during hail events occurring on 8 February 2018, 14 December 2018, and 24 October 2020, as shown in Figure 1. Each time Argentinian citizens collected hail, they took a picture with their hands or other objects as a size reference, stored them in their fridges ($-13\text{ }^{\circ}\text{C}$), and then contacted us to recover the samples. This hail collection and conservation procedure, “Cosecheros de granizo Córdoba,” started in October 2018. Once a hail event was reported, the team drove to the location, then recorded the location of the hail fall, the time of collection, and if it rained before, during, or after the fall. The name of the person who collected the sample and who signed the hail sample ownership transfer for the laboratory analysis was recorded. Hail samples were then transferred to a thermally reinforced cooler before moving to a laboratory cold chamber to prolong the crystallographic structure for further analysis. For this present study, the focus was on the location, time, and size of the 48 hail samples collected on 8 February, nine samples on 14 December, and four on 24 October. Sizes ranged from 1.3 cm on 14 December and 24 October to 17 cm diameter hail on 8 February (referred to as “Victoria’s gargantuan hail” [33] and “El Coloso Victoria” [34]), as shown in Table 1.

Additional locations of hail fall during these three events were found through social media platforms such as Twitter, Facebook, and local newspapers online. As seen in Table 1, most of the collected hail events also had reported hail on these media platforms. In looking back at these events, satellite-based tracking of these storms, as detailed below, provided additional times and regions to focus on to search for mentions of hail on social media. Through this approach, two additional hail reports were found on 8 February and two for

24 October that provided verified hail at a given location and time, but most lacked reliable size information.

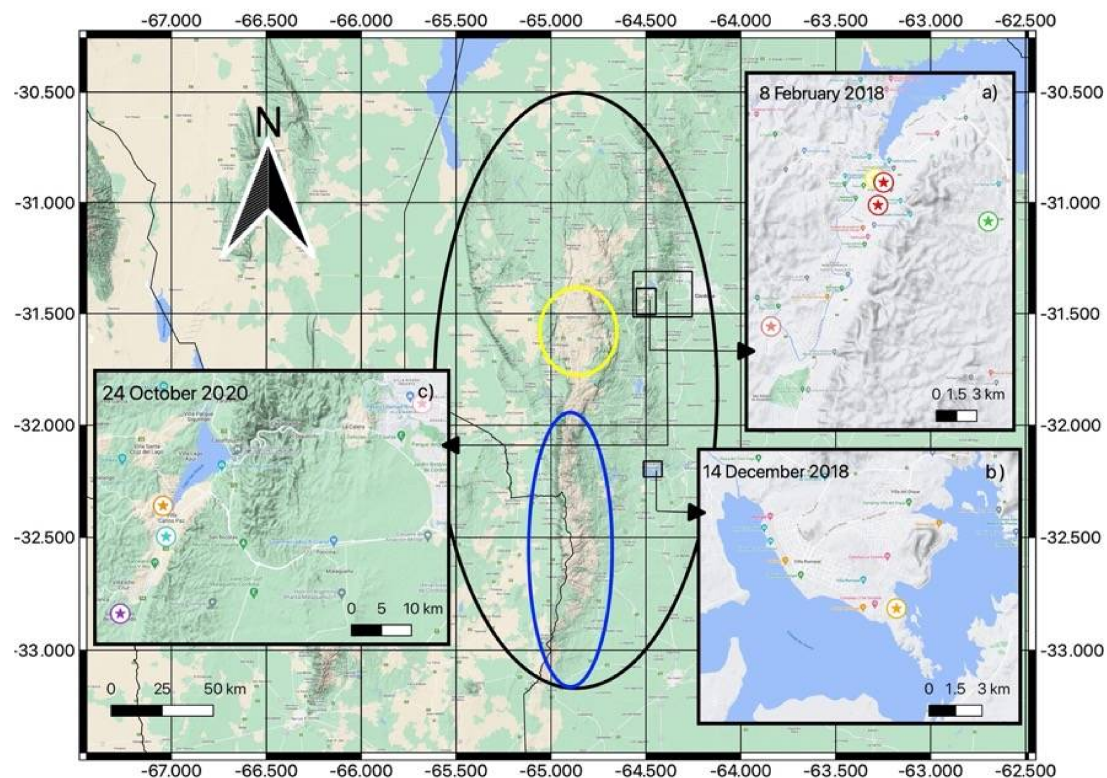


Figure 1. Map showing the “Sierras de Córdoba” (circled by a black marking) with a blue circle surrounding the “Sierras de Comechingones” and a yellow circle surrounding the “Sierras Grandes” and locations where hail reports were available. Each star with its respective color is associated to each hail report for (a) 8 February 2018 at 18:50 UTC (light coral), 19:20 UTC (red), 19:30 UTC (yellow), 19:45 UTC (lime green); (b) 14 December 2018 at 02:20 (orange); and (c) 24 October 2020 at 18:20 UTC (turquoise), 18:32 UTC (dark orchid), 18:35 UTC (dark orange), 19:27 UTC (light pink).

Table 1. Hail event information corresponding to storms on 8 February 2018, 14 December 2018, and 24 October 2020 in the Córdoba Province in Argentina. Social media and local news included Twitter, local news in Villa Carlos Paz (VCP) and nearby cities, and the Citizen Science Program “Cosecheros de Granzio” database.

Date	Time of Hail Event (UTC)	Sample Size	Location	Coordinates	Information Source		Maximum Hail Size (cm)
					Sample Collected	Social Media /Local News	
8 February 2018	18:50	None	Icho Cruz	−31.470844, −64.541380	No	Yes	5
	19:20		Calle San Lorenzo, VCP	−31.422844, −64.497452	Yes	Yes	17
	19:20	48	Calle Tupungato, VCP	−31.430425, −64.499612	Yes	Yes	8
	19:30		Calle Tokio, VCP	−31.421580, −64.500763	Yes	Yes	4
	19:45	None	San Nicolás	−31.435851, −64.456595	No	Yes	None

Table 1. Cont.

Date	Time of Hail Event (UTC)	Sample Size	Location	Coordinates	Information Source		Maximum Hail Size (cm)
					Sample Collected	Social Media /Local News	
14 December 2018	02:20	1	Villa del Dique	−32.201393, −64.452606	Yes	Yes	8
	03:00	8	Córdoba, Córdoba	−31.4201, −64.1888	Yes	No	1.3
24 October 2020	18:20	4	VCP	−31.434703, −64.504108	Yes	Yes	3
	18:32		San Antonio de Redondo	−31.492307, −64.544306	No	Yes	1.5
	18:35		VCP N	−31.411644, −64.506675	Yes	No	1.5
	19:27	None	Villa Allende	−31.335028, −64.279508	No	Yes	1.5

2.2. Convective Storm Identification and Tracking

2.2.1. Geostationary Satellite

To identify and track each storm, specific channels from the geostationary satellite GOES-16 were used. This satellite has a spatial resolution ranging from 0.5 km for the 0.64 μm visible channel to 2 km for channels greater than 2 μm . Data are available every 15 min for case studies in 2018 and every 10 min for the case in 2020. Channel 13 (10.3 μm) was used to infer the relative updraft strength by calculating the temporal derivative of the brightness temperatures [35–37]. Channel 11 (8.4 μm) was also chosen to infer storm strength based on the relationship previously established by Müller et al. (2019) [31], where brightness temperature cooling rates of convective clouds correspond to updraft strengths. Cloud-top cooling rates lower than -4 K in 15 min are associated with a weak cloud growth, while cooling rates of -8 K and smaller in 15 min are associated with a strong updraft that can lead to more intense storms [35,37].

Differences between Channel 11 and Channel 14 (11.2 μm) were used to look at the cloud-top ice crystal sizes present in the cloud. High positive values are associated with small ice crystals and low positive values with larger ice crystals [38]. When used in a tri-spectral differences analysis, subtracting the difference between Channel 14 and Channel 15 (12.3 μm) from the Channel 11–14 difference provides information on the cloud phase, enabling us to infer the rate of change of the mass of ice crystals in the system. Positive values of the tri-spectral difference are associated with ice crystals and negative values with water droplets [38,39].

Parallax was accounted for in the analysis of satellite products by adding the cloud top height to the equatorial and polar radius when calculating latitude and longitude for each pixel. Cloud top height data for 24 October were taken from the cloud top height algorithm from GOES-16, which uses Advanced Baseline Imager infrared channels. These data were unavailable for the 8 February and 14 December cases, so cloud top height for the first two cases (15, 16 km, respectively) was estimated using soundings, radar imagery, and brightness temperatures, while the 24 October cloud top height (12 km) was found using the GOES-16 cloud top height product for full disk.

The goal was to infer evolving storm intensity and investigate the temporal evolution of the satellite-derived parameters leading up to the hail and thus to seek possible hail fall signatures (e.g., [25]). The first step was to objectively define a convective core associated with the hail-producing storm. To do so, a minimum in brightness temperature was identified spatially and temporally near each hail report (Figure 2a). Through GOES-16 loops, the core was tracked visually back in time prior to hail events and forward in time

after the hail fell. Thus, the spatial and temporal analysis domain was defined by this visual inspection. An example of this manually defined spatial domain is shown in Figure 2b.

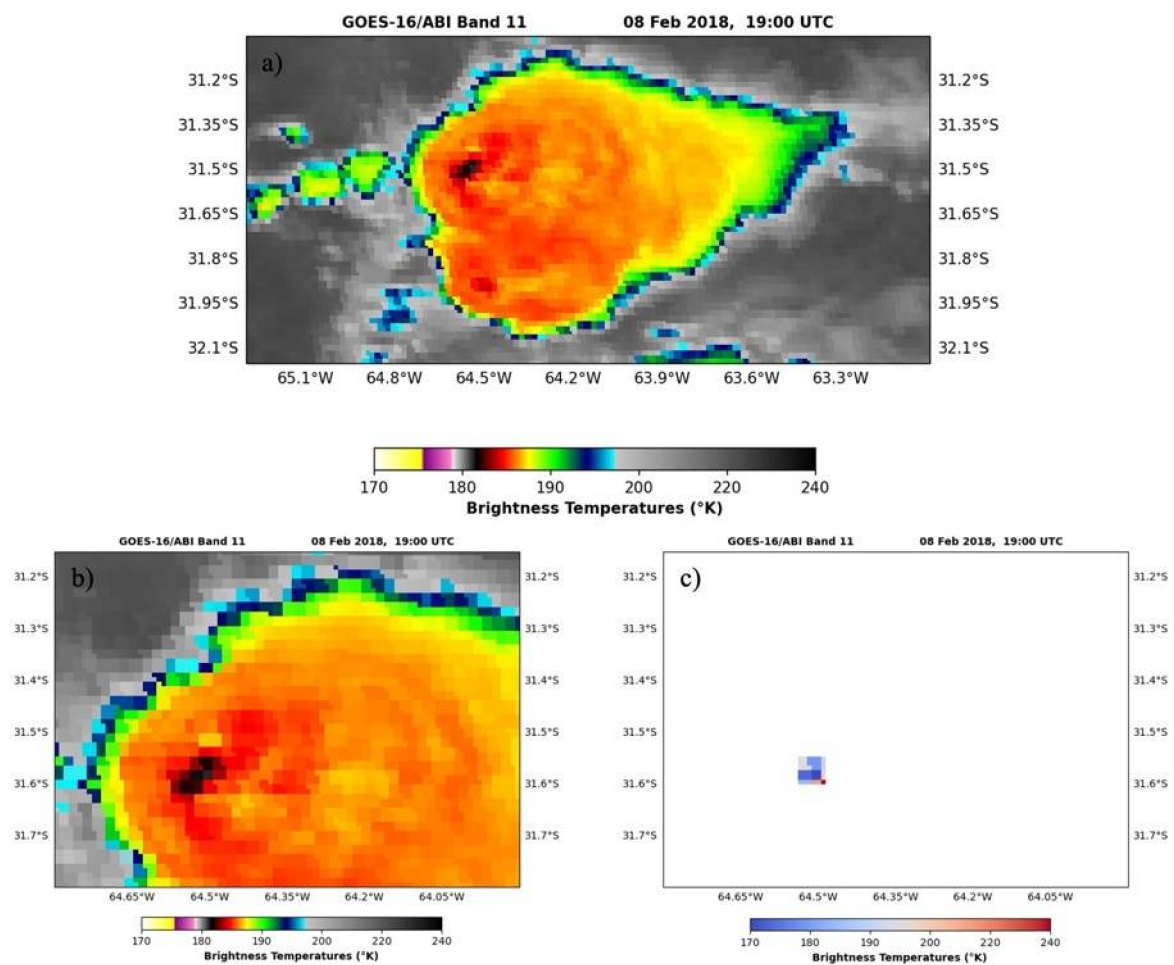


Figure 2. (a) GOES-16 Channel 11 from 19:00 UTC on 8 February 2018; (b) convective core search area; (c) brightness temperatures within the objectively identified convective core.

To objectively compute changes in brightness temperatures and other satellite-based trends associated with this convective core, the location of the minimum brightness temperature was determined from Channel 11 at each time step within the defined spatial domain (Figure 2b). Then, inflection points were calculated from the lowest brightness temperature pixel to the image's northern, southern, western, and eastern bounds (a modified version of the method used in Borque et al. (2020) [32]). The inflection point was found by calculating the second derivative of every brightness temperature in each of the four directions starting from the minimum brightness temperature. The first sign change was identified (inflection point) as the convection core boundary within the pre-defined bound. The pixels contained within these bounds (including the pixel containing the inflection point's value) were then defined as the convective core (Figure 2c) to continue with the satellite analysis, with all other pixels excluded, which differed from the method in Ribeiro et al. (2019) [25], which relied on a single brightness temperature threshold for their case study. Brightness temperatures in both Channels 11 and 13 and satellite-derived trends additionally using Channels 14 and 15 (updraft strength, ice mass, and particle size of ice crystals) were then computed within this convective core and correlated in space and time with hail reports. The hail reports associated with the start time of the satellite data file was compared to the previous time to look for trends leading to the hail report. In a few instances, when the hail

was reported at the exact start time of the satellite file, then the previous two times were compared to look for trends prior to the hail fall for potential nowcasting applications.

2.2.2. Radar

Radar data used for this project came from the operational C-band dual-polarization Doppler Córdoba radar (5.4-cm wavelength), RMA1. This radar system was designed and manufactured by INVAP–South America and operated by the National System of Meteorological Radars for Argentina’s “Sistema Nacional de Radares Meteorológicos” (SINARAME). This project had access to three surveillance elevation angles (0.5° , 1.0° , 1.5°) consistently across the three events, available every 10 min. For this analysis, horizontal reflectivity and Doppler velocity were used to determine the storm mode of the hail-producing cases. Absolute calibration of the data varied for the cases, but differences in the magnitude of the radar variables across cases were not relevant for the analysis.

2.2.3. Environmental Data and Storm Warnings

Environmental data are used to characterize the pre-convective conditions under which the hail-producing storms form. Isobaric charts at 850 and 500 hPa at 12:00 and 00:00 UTC for South America were available from the University of Wyoming archive [40]. Operational soundings were used mainly from Córdoba Airport at 00:00 and 12:00 UTC from an online source in Argentina provided by the University of Wyoming online portal [41]. Large-scale daily composites of 850-hPa specific humidity anomalies were available from the Physical Science Laboratory NCEP/NCAR reanalysis datasets [42]. Official storm warnings can be accessed through the official governmental page of the National Meteorological Service of Argentina (SMN) within 365 days after being issued or after this time limit by request. For each case study, these warnings were available through the official SMN Twitter account to compare their forecast with the analysis for each case. Finally, surface station observations and soundings from Córdoba Airport and Santa Rosa Airport at 12:00 and 22:00 UTC collected during the RELAMPAGO field campaign were used for the 13 December case analysis [43].

3. Results

3.1. 13–14 December 2018 MCS

3.1.1. Environmental Setting

This case started on the evening of 13 December 2018 to the west of the RELAMPAGO field campaign domain (located along the eastern edge of the SDCs near Córdoba city). Convection initiated over the high plains of San Luis (west of the Sierra de Comechingones, blue circle in Figure 1; maximum elevation 1.0 km) around 22:00 UTC, then moved eastward toward the Sierras Comechingones, a mountain in the SDCs that can reach up to 2.8 km (Figure 1; blue circle). The first verified hail report (8 cm in diameter) occurred at 02:20 UTC over Villa del Dique (Figure 1b), a town at an elevation of ~550 m located 110 km south of Córdoba city (Figure 1). As the hail-producing storm continued northeastward, hail reaching 1.3 cm in diameter (Table 1) was reported at 03:00 UTC in the city of Córdoba, in addition to flooding and frequent lightning [15].

The 500-hPa charts at 12:00 UTC 13 December and 00:00 UTC 14 December (Figure 3) show the passage of a mid-level trough over the Andes leading up to the hail event. The response at 850 hPa is troughing to the lee of the Andes; a set up previously shown to be associated with deep and wide convective systems near the SDCs (e.g., [19,23,44]). Composite anomalies of 850-hPa relative humidity (Figure 4) for 13 December showed an area of anomalously high moisture in central Argentina. The 850-hPa wind at Córdoba Airport (SACO station in Figure 5) was 25 kt out of the north at 12:00 UTC, suggesting this anomalously high moisture was ushered in from the north. This pattern is consistent with previous studies linking moisture transport via the SALLJ to convective activity near the SDCs (e.g., [21,45–47]).

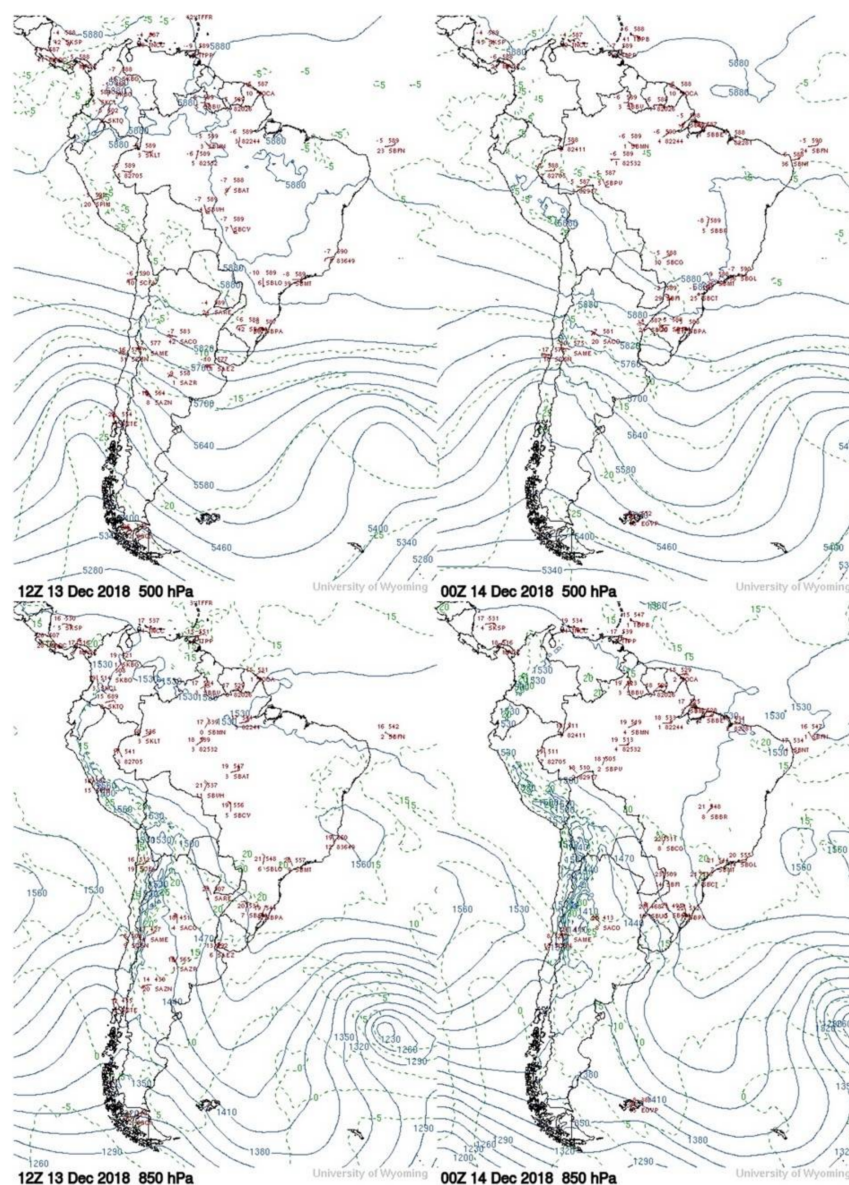


Figure 3. Isobaric chart at 500 and 850 hPa for 12:00 UTC on 13 December 2018 and 00:00 UTC on 14 December 2018 from the University of Wyoming [40]. Solid blue lines show isobars; dashed green lines show the isotherms; and red text are surface station observations.

The 12:00 UTC 13 December sounding from Córdoba Airport (Figure 5) showed a peak northerly flow of 25 kt at 850 hPa consistent with the SALLJ. These moist low levels are capped by dry large-scale subsidence (westerly flow seen at 500 hPa on Figure 5) induced by the mid-level trough approaching from the west (Figure 3). By 00:00 UTC on 14 December, there was increased elevated CAPE reaching 2308 J/kg, a well-mixed boundary layer, and reduction in the capping inversion; a scenario favorable for vigorous and widespread convection to develop in this region (e.g., [19,23]). Note that at this time, the 30-kt SALLJ core is elevated, occurring closer to 700 hPa (as described in more detail in Sasaki et al. (2022) [21]), with a potential impact on wind shear and storm evolution.

Overall, the mid-level trough crossing the Andes, strong low-level jet, large-scale subsidence off the Andes, and large CAPE values are key ingredients that made this environment favorable for deep convection and similar to environmental conditions favorable for organized convection [23] and hail [15] in this region. The SMN, through their official Twitter account, forecasted on 12 December at 0500 LST the potential for intense rainfall for the morning of 13 December extending to 14 December with rainfall reaching 50 and

150 mm for the southeast area of Córdoba, but no specific mentions of hail for that evening. The RELAMPAGO field campaign forecast team, in close coordination with SMN forecasters, discussed the conditions favorable for convection initiation, then upscale growth and possible hail around 21:00 UTC, although the exact location and timing of the MCS and hail was uncertain.

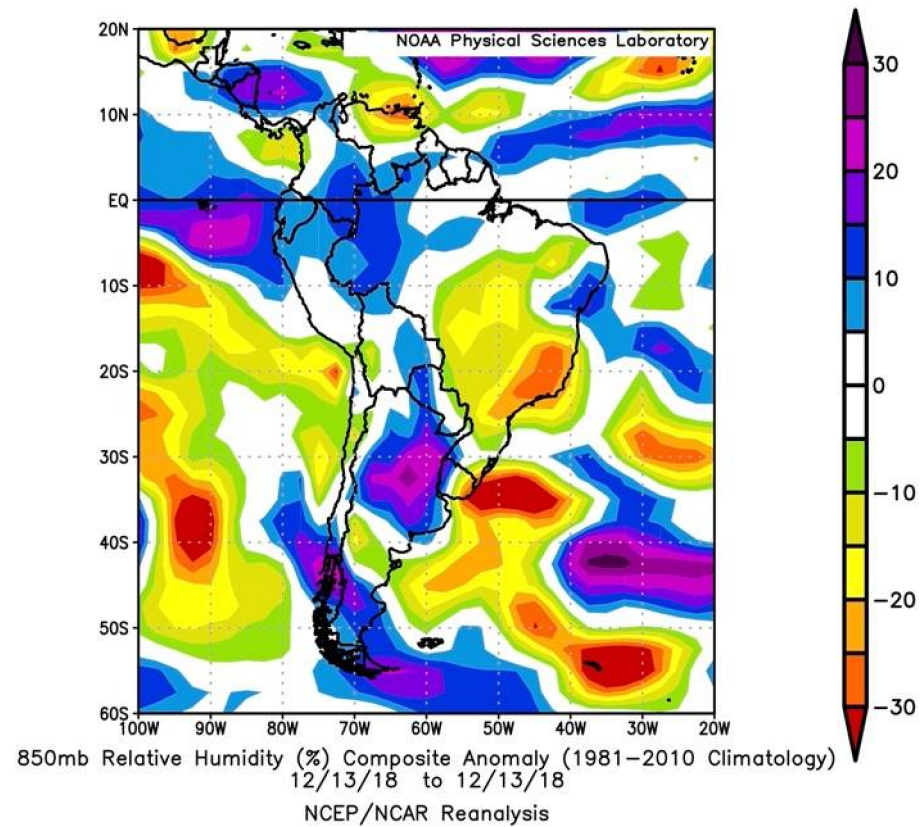


Figure 4. Relative humidity composite anomaly at 850 mb for 14 December 2018 [42].

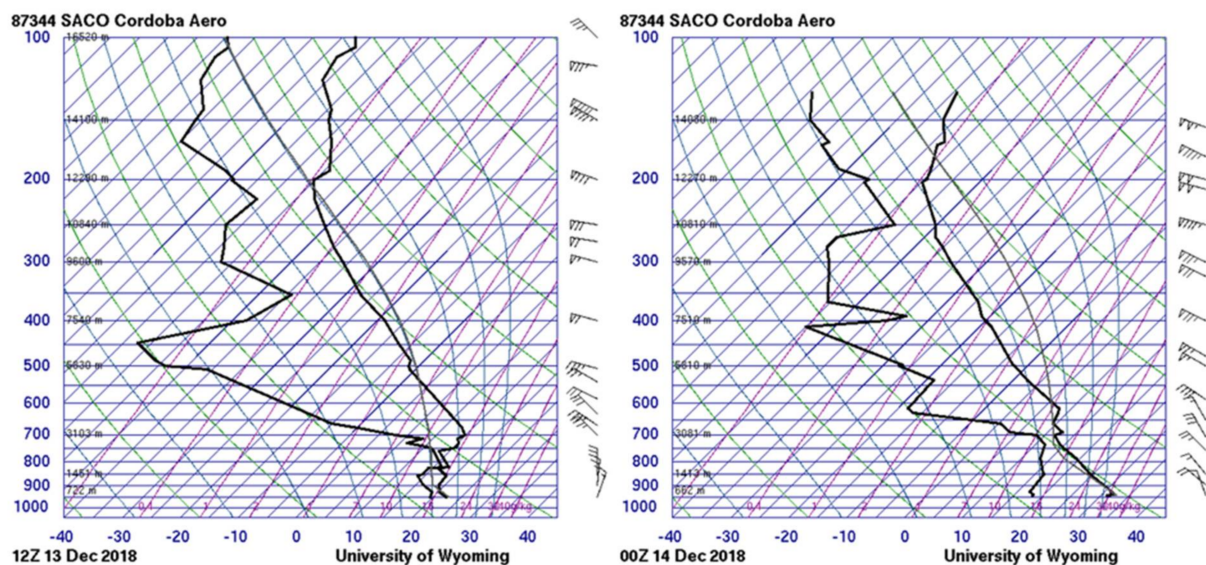


Figure 5. Atmospheric soundings from Córdoba Airport in Córdoba Province, Argentina at 12:00 UTC on 13 December 2018 and 00:00 UTC on 14 December 2018 [41].

3.1.2. Convective Characteristics

Figure 6 shows the general temporal evolution of the 13–14 December storm as viewed from GOES-16 Channel 13 brightness temperatures. The white box includes the area over which the convective core was tracked before, during, and after the reported hail fall (as described in Section 2) until it merged with a different cell. The 8-cm hail report analyzed in this case occurred at 02:20 UTC in Villa de Dique (Figure 1b). After the cells merged following this initial hail report, small hail (over 0.5 cm) was reported in the city of Córdoba at approximately 03:00 UTC. Limited hail samples, especially earlier in the event over the mountains, can be attributed to the fact that the storm developed during the night, which limited the number of people able to record the event, and lower population densities near the higher peaks of the SDCs.

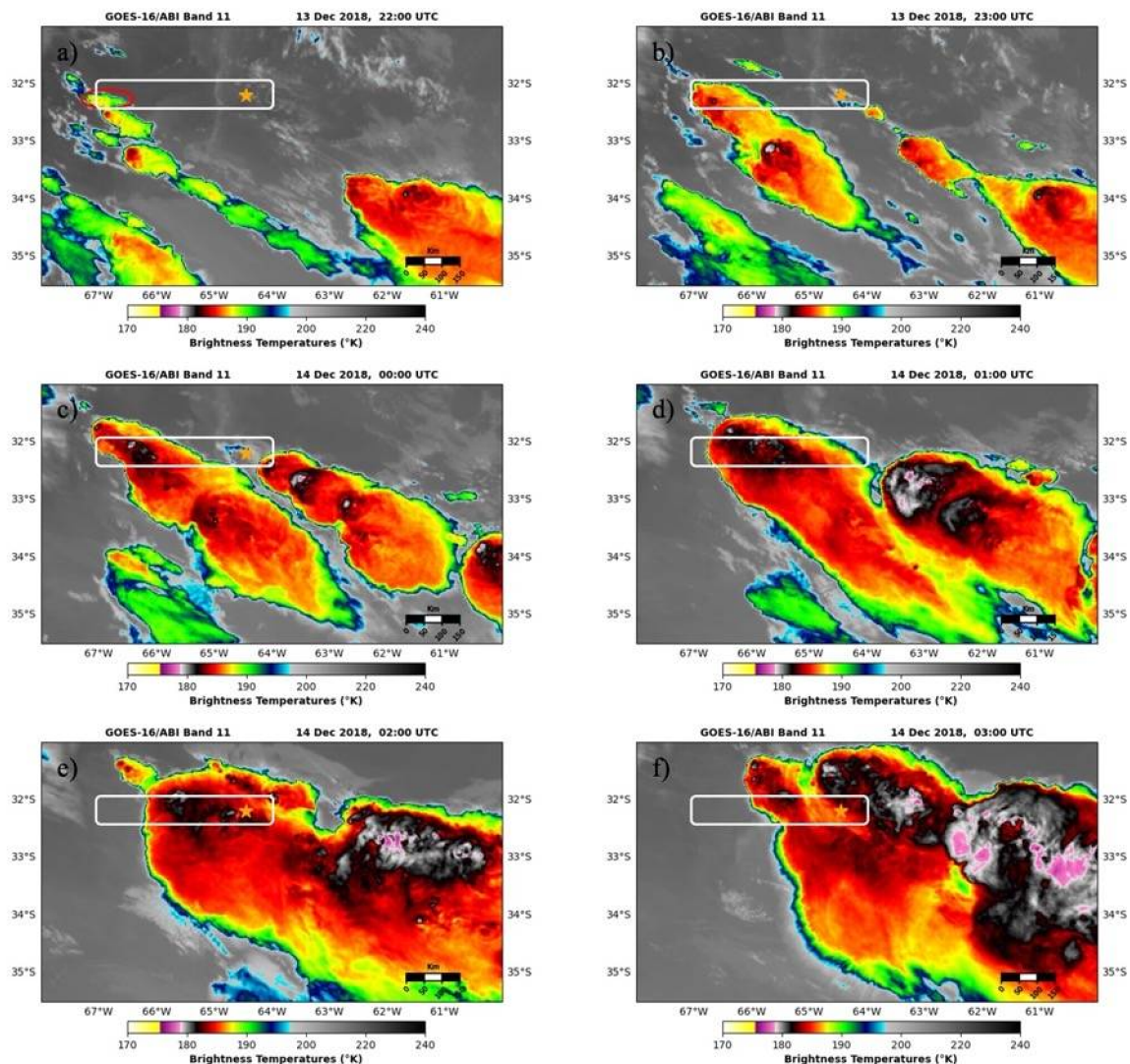


Figure 6. Subfigures (a–f) are figures in one-hour intervals from GOES-16, Channel 11, showing the convective system responsible for hail fall (marked by a red circle at 22:00 UTC) studied on 13 December 2018. White rectangle highlights the area of interest for convective core tracking. As shown in Table 1, these images were just before and during the recorded hail events. Orange star is associated with the hail report at 02:20 UTC in Villa del Dique on 14 December 2018.

Based on surface observations across the Córdoba Province (not shown, [48]), there was a switch in wind direction on 13 December at 22:00 UTC south of the Córdoba Province from northeast to southeast, separating relatively warmer moist air from the north with a colder air mass to the south. The convection that later produced hail during this case

formed along the western extent of the cold front over the high plains of San Luis Province around 22:00 UTC (Figure 6a), and eventually evolved into a MCS over the high terrain. The cell that produced the hail report at 02:20 UTC later merged with another cell before producing 1.3 cm hail in Córdoba city. While tracking the convective core (Figure 6), a strengthening was observed after it crossed the Sierras de Comechingones at 00:00 UTC, followed by multiple warming and cooling episodes indicating the strengthening and weakening of the updrafts within the MCS. At 02:00 UTC, 20 min before the hail report in Villa del Dique, there were enhanced-V and Above-Anvil Cirrus Plume (AACP) signatures at 32.28° S, 64.59° W, which previous literature has suggested could be indicative of severe weather (e.g., [49]).

The RMA1 radar reflectivity image just before the time of the hail report (Figure 7) showed that the hail event was associated with widespread echo over the mountains to the southwest of Córdoba, and that the convective core identified from parallax-corrected satellite data (gray box in Figure 7) was indeed associated with this hail event. Note that this hail-producing storm was attenuated in the C-band RMA1 data due to the intense convection that formed closer to the radar, making it challenging to nowcast this hail event from the operational radar data alone. The region of high reflectivity that can be observed in Figure 7, north of Villa del Dique (Figure 1c), is an independent cell that hailed at 03:00 UTC at Córdoba City, and for this reason, was not included in further analysis in this study.

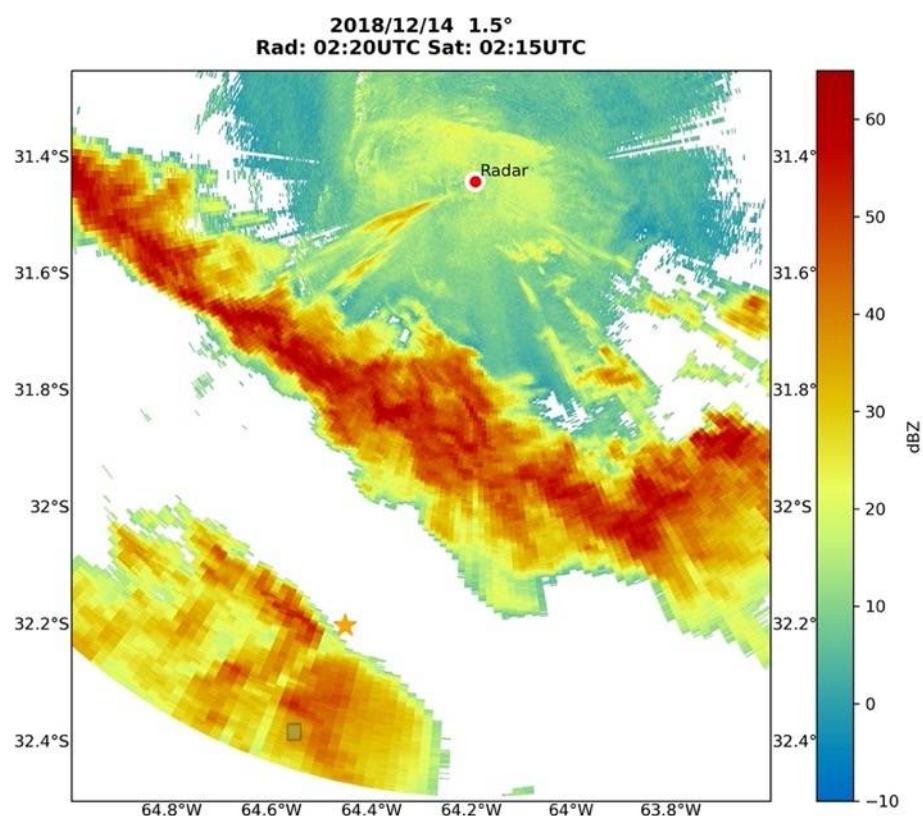


Figure 7. Reflectivity images from RMA1 radar showing the MCS at 02:15 UTC on 23 December 2018 and location where hail fall was reported (orange star). The grey box is the satellite-tracked core, which is associated with the MCS producing the hail marked by the orange star with an area of high reflectivity. This radar reflectivity image was from an elevation angle of 1.5 deg.

3.1.3. Temporal Trends in Satellite Data

The previous discussion suggests variations in the intensity of the evolving MCS leading up to the hail report on 14 December. This section focuses on an objective analysis of the temporal evolution of this MCS to search for patterns linking satellite-derived trends

to the verified hail at the ground. Recall that the convective core was identified using the minimum brightness temperature in the white box of Figure 6 through methods described in Section 2. Figure 8 shows the results of the satellite-based objective analysis for times leading up to, during, and after the 02:20 UTC 8-cm reported hailstone in Villa del Dique.

Brightness temperatures from Channel 13 in the convective core (Figure 8a) showed a gradual decrease of 212 K to 193 K from 22:30 to 23:30 UTC, a cooling rate of -19 K/h, reaching colder temperatures than the tropopause (198 K) based on available sounding from 00:00 UTC on 14 December from Córdoba Airport (Figure 5). Then, brightness temperatures remained within an average of 198 K (i.e., tropopause temperature) with a standard deviation of 3 K between 23:30 and 03:00 UTC, times in which hail was collected. This trend can be linked back to the evolution of this MCS in Figure 6; the convective cell initially strengthened rapidly, then remained relatively steady for a couple of hours, while other nearby cells appeared in the proximity of the tracked convective core. During this latter period (23:30 to 02:00 UTC), the tri-spectral analysis showed positive values staying within an average of 3 K (Figure 8c). During the same time, the ice crystal size analysis was within an average of 5 K (Figure 8d), indicating the presence of small ice crystals in the cloud during the reported hail periods [36].

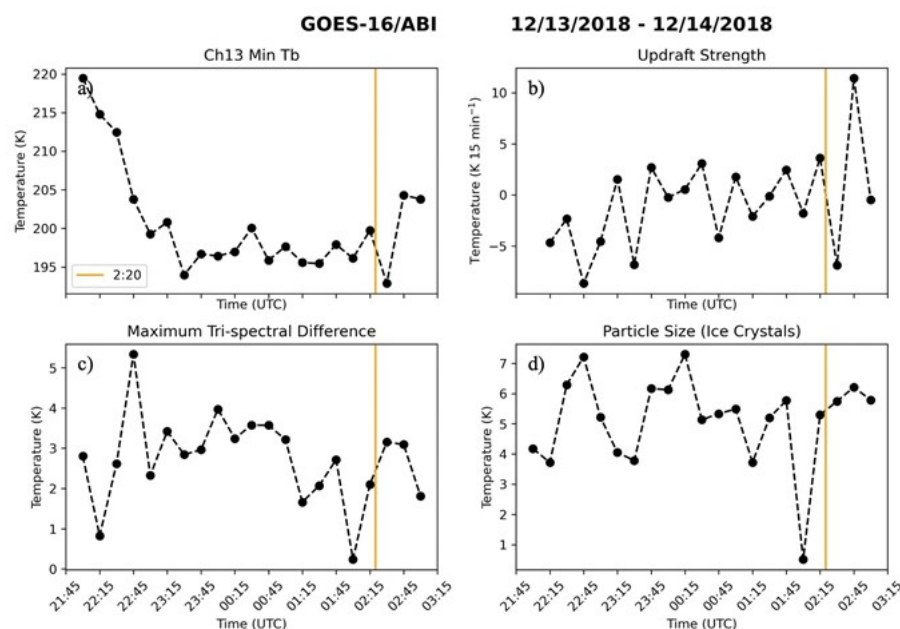


Figure 8. Temporal variation for 13–14 December 2018 of (a) local minimum $10.35\ \mu\text{m}$ Tb (K) as a proxy for storm strength; (b) temporal trend of $10.35\ \mu\text{m}$ Tb (K min 15) to identify cooling and warming episodes related to updraft weakening and strengthening, respectively; (c) maximum tri-spectral difference (K), which indicates the mass of ice crystals through full depth of cloud (positive values, presence of ice crystals; negative values, presence of water droplets); and (d) maximum difference between $8.5\text{-}\mu\text{m}$ and $11.2\text{-}\mu\text{m}$ Tb (K), which provides the predominant ice crystal size in the cloud (greater positive values, smaller ice crystals; smaller positive values, larger ice crystals). Orange line marks the time of hail fall. Data used in this analysis correspond to 15 min intervals starting from 21:45 UTC.

Regarding the updraft, a slight weakening of the updraft was inferred 15 min prior to the 8-cm hail report at 02:20 UTC because the brightness temperatures increased 3.6 K in 15 min (Figure 8b) leading up to the hail. Over the same time, both the tri-spectral differences (Figure 8c) and the concentration of small ice crystals (Figure 8d) increased just prior to the hail report. This signature was not unique through the time series because there were similar patterns observed earlier during the developing stages that could be linked to non-verified hail events in this region. These results are partially consistent with the analysis by Ribeiro et al. (2019) [25] for clouds with large vertical development and

increases in small ice crystal concentration in the cloud prior to reported hail. In summary, the satellite-based temporal analysis for the 14 December MCS case showed a gradual decrease in brightness temperatures until the cell reached temperatures near and above the tropopause. After a strong intensification of the convective cell, there were more subtle changes in brightness temperature as nearby cells grew and decayed and the MCS, as a whole, moved over the mountains. In the 15 min prior to the hail report, a slight increase was observed in the brightness temperatures associated with a slightly weakening updraft, along with the notable presence of an increase in ice mass in the cloud.

3.2. 8 February 2018 Supercell

3.2.1. Environmental Setting

On the evening of 8 February 2018, two distinct cells developed in two different regions in the Córdoba Province: a “southern” cell that became convective over the San Luis Province plains to the southwest of the Sierras Comechingones (Figure 1; southwest of the blue circle) and an initially smaller “northern” cell that developed east of the Sierras Grandes (Figure 1; yellow circle), a mountain range that reaches an elevation of 2.1 km. This northern cell continued to evolve rapidly, producing the five confirmed hail reports mentioned in Table 1 and analyzed in this section, while the southern cell, after it was south of the Sierras de Comechingones (Figure 1; blue circle), started merging with the northern cell before dissipating.

Isobaric charts for this event (Figure 9) show zonal flow at 500 hPa located south of the SDCs and a 500 hPa trough off the west coast of South America moving over Patagonia, which was broader and farther south compared to the deeper mid-level trough that moved over the Andes during the 13–14 December event. Consequently, the leeside 850-hPa troughing occurred south of the Córdoba domain. Relative humidity composite reanalysis (Figure 10) showed a lack of a moisture anomaly in central Argentina, which differed from that seen on 14 December. The sounding in Figure 11 showed a lack of a low-level jet and overall drier low levels compared to the 14 December case. Wind direction at 500 hPa also differed from observations on the 14 December case, having a southwesterly flow of similar speeds to the northwesterly flow observed during the 14 December case. Mixed-layer CAPE values were only 11.67 J/kg at 12:00 UTC (MUCAPE 300 J/kg; [33]), which was not especially favorable for convection over Córdoba city. Additionally, a capping inversion was observed at the 700-hPa level at both times, limiting surface-based convection near Córdoba in an already relatively dry lower atmosphere. This suggests that the 12:00 UTC Córdoba sounding is not an appropriate indicator of local conditions over the nearby mountains during this case. Model-simulated thermodynamic profiles from this case [33] suggested a weaker inversion located over the SDCs, and an increase in instability as the boundary layer moistened by 20:00 UTC.

Overall, the lack of LLJ during this case indicates a lack of large-scale moisture transport, and a lack of large-scale forcing is supported by the trough at 850 hPa at 12:00 UTC located farther south near Patagonia, suggesting that local forcing from upslope flow was responsible for convective initiation on 8 February. SMN forecasters discussed on 8 February via Twitter that conditions were favorable for strong rains, isolated storms, and cloudburst of intense rain, with no mention of forecasted hail for the region of Córdoba Province.

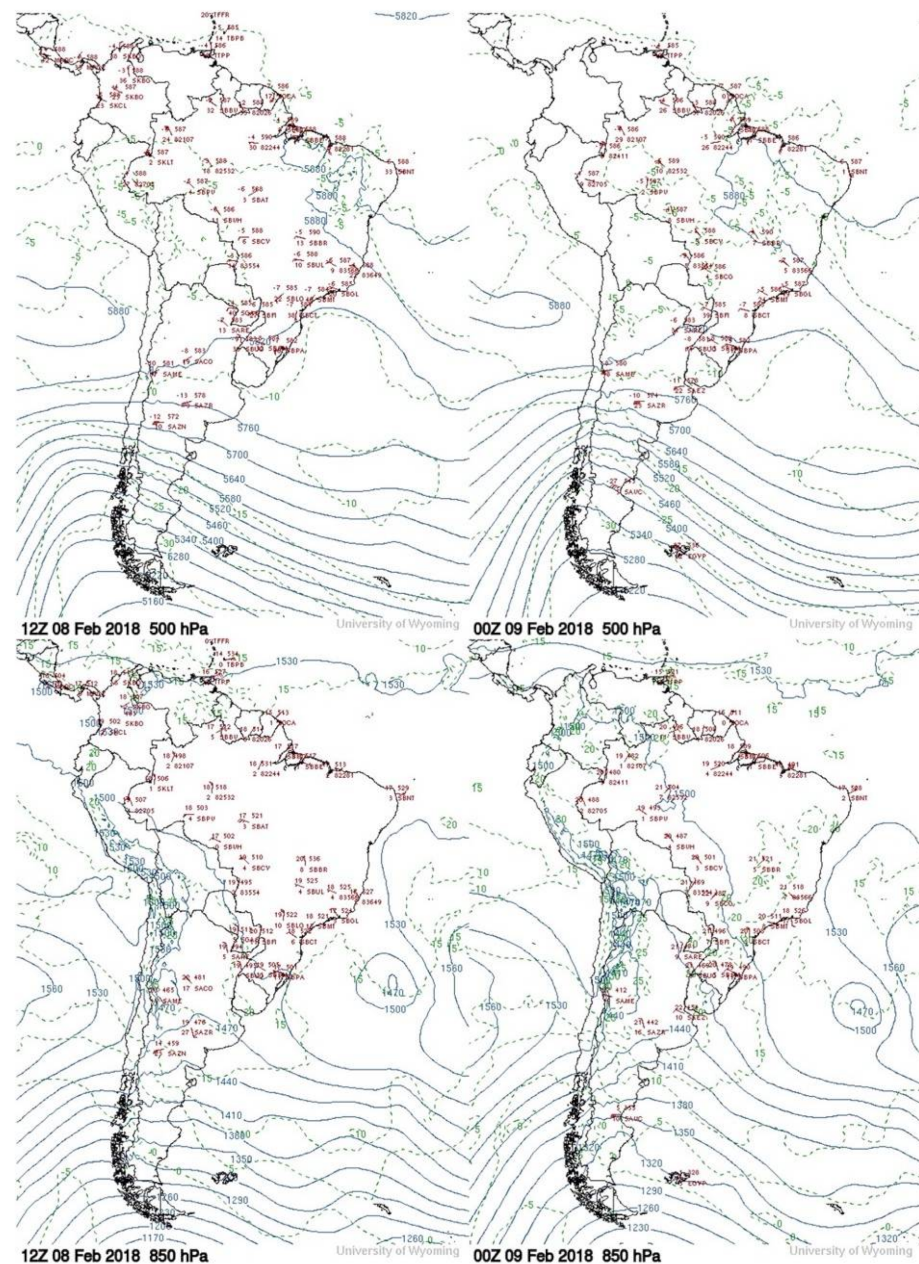


Figure 9. Isobaric charts at 500 and 850 hPa for 12:00 UTC on 8 February 2018 and 00:00 UTC on 9 February 2018 from the University of Wyoming [40]. Solid blue lines show isobars; dashed green lines show the isotherms; and red text are surface station observations.

3.2.2. Convective Characteristics

Figure 12 at 18:00 UTC shows the satellite-view of the evolving convection during this case from the Channel 13 brightness temperatures. In this plot, the red box highlights the “southern” cell (no hail reports), the white box highlights the northern cell (hail reports ranging from 4 to 17 cm in diameter), and the black box shows the convective core analysis bounds for the northern cell. These plots show that for the northern cell, a gradual decrease in brightness temperatures was observed before the first hail event. The northern cell became convective at 18:00 UTC and evolved east of the Sierras Grandes whereas the southern cell developed over plains in the San Luis Province. The southern cell was more spatially extensive than the northern cell, but it did not have as low brightness temperatures as the northern cell (southern cell showed 210–215 K vs. northern cell showing 200 K).

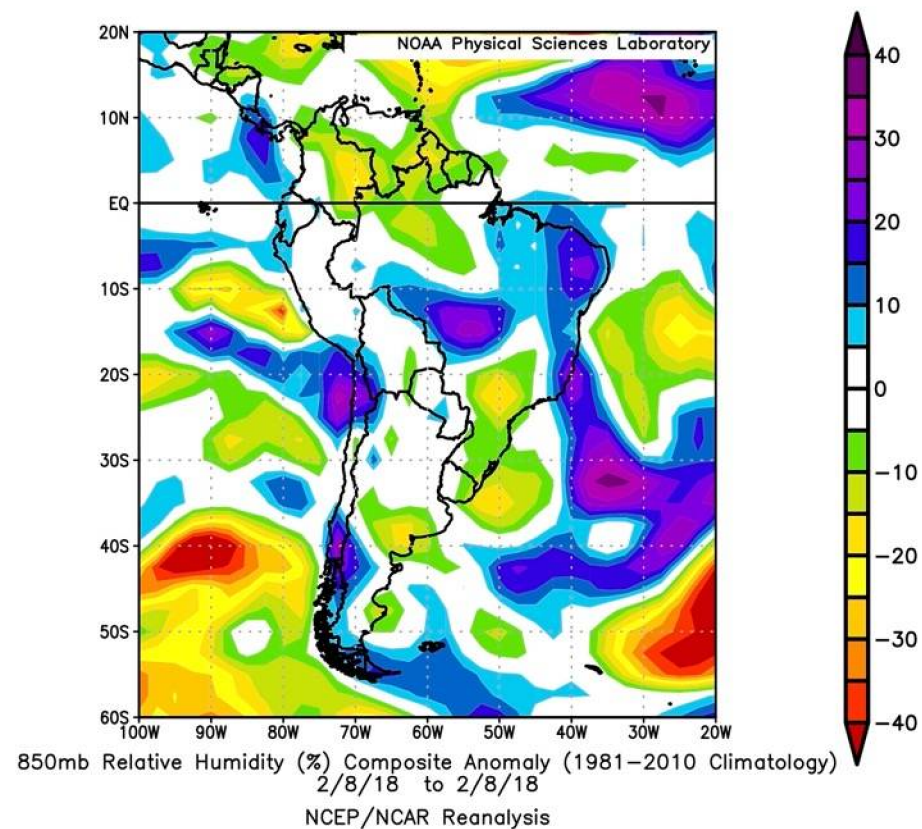


Figure 10. Relative humidity composite anomaly at 850 mb for 8 February 2018 [42].

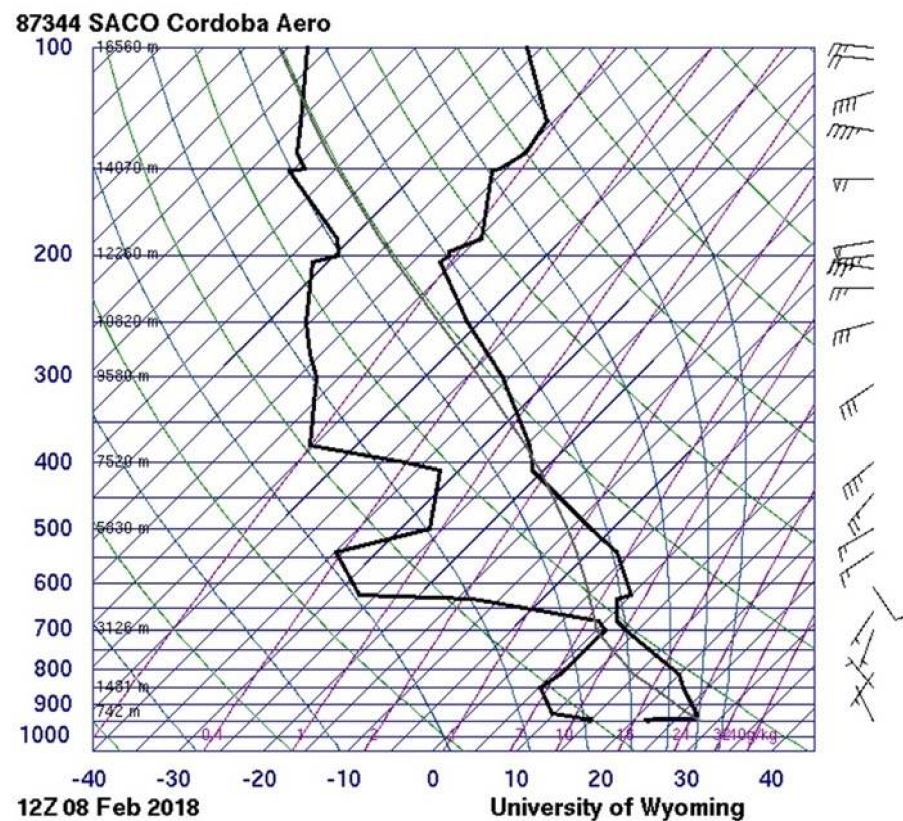


Figure 11. Atmospheric soundings from Córdoba Airport in Córdoba Province, Argentina at 12:00 UTC on 8 February 2018 [41].

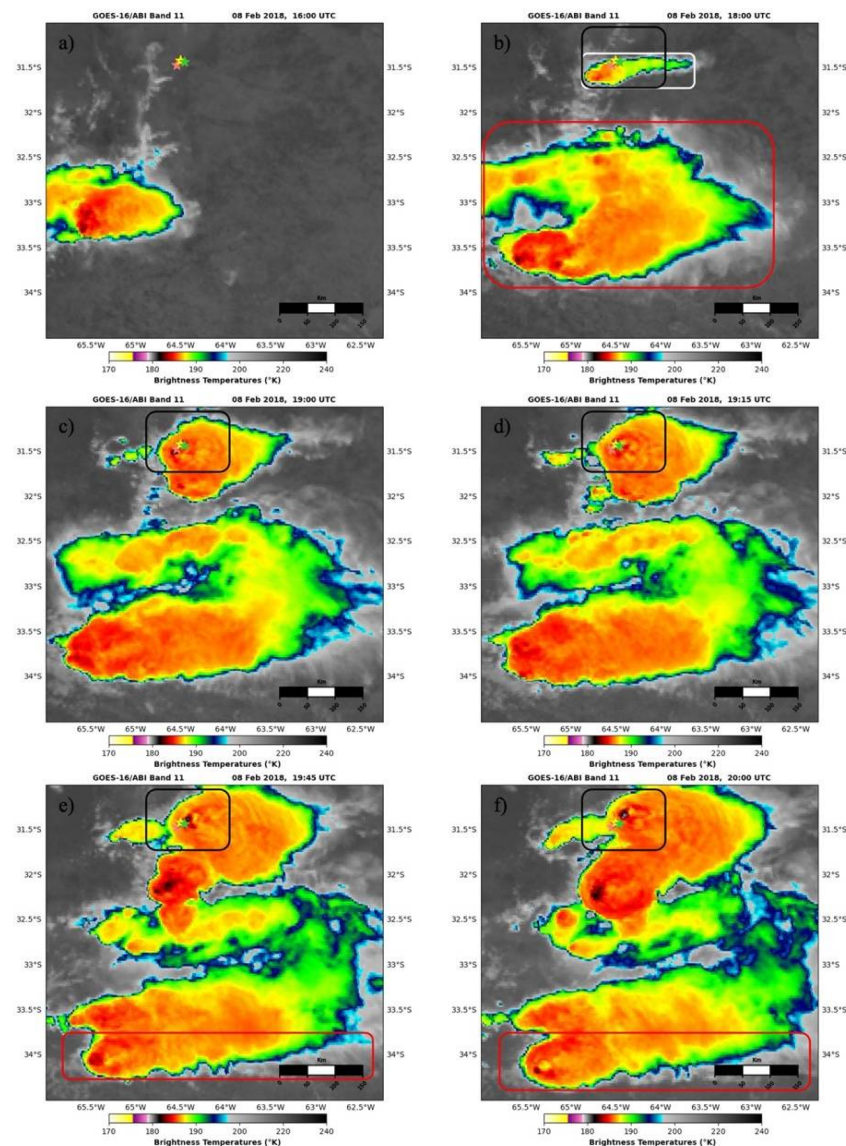


Figure 12. Subfigures (a–f) are figures in one-hour intervals from GOES-16, Channel 11, showing the two convective systems studied on 8 February 2018. Red box highlights the “southern” cell, the white box highlights the northern cell, and the black box shows the convective core analysis bounds for the northern cell. As shown in Table 1, these images were just before and during the recorded hailstorms. Each star is associated with each hail report: 18:50 UTC (light coral), 19:20 UTC (red), 19:20 UTC, 19:30 UTC (yellow), 19:45 UTC (lime green) at Icho Cruz, Calle San Lorenzo, Calle Tupungato, Calle Tokio, San Nicolás, respectively.

This observation suggests that the southern cell did not have as deep a vertical development as the northern cell and therefore, it was assumed that it had lower chances of producing hail, although there was no confirmation of whether this cell produced hail as it occurred in an area with low population density and at the range limit of the RMA1. Similar to the 14 December case, the convective core of the northern cell was identified and tracked, observing multiple warming and cooling episodes that indicated the strengthening and weakening of the updraft leading up to the hail reports at 18:50, 19:20, 19:30, and 19:45 UTC (Figure 1a). Enhanced V and AACPs signatures were also observed previous to each hail report (e.g., at 31.40° S, 64.43° W at 19:15 and 19:45 UTC and 31.31° S, 64.34° W at 20:00 UTC), which can be indicative of the severe weather confirmed in this case. Additionally, as observed in the 14 December case, the overshooting top extended

above the tropopause (215 K), which was confirmed by the sounding at Córdoba Airport at 12:00 UTC (Figure 11).

RMA1 radar reflectivity during this event and radial velocity data (not shown) revealed that the convective cell responsible for the verified hail event in Villa Carlos Paz (red stars in Figure 13) was a supercell at 19:20 UTC right before the hail was reported. This northern convective cell was only tracked until the last hail report recorded at 1945 UTC in San Nicolas. There was no other intense convection between this storm and the radar, which will cause less attenuation (unlike the 14 December case), and a strong core exceeding 60 dBZ was observed around the time of the first hail report. An overlay of convective core pixels from Channel 11 (gray box in Figure 13) over the radar reflectivity data showed close alignment between the convective core identified in satellite images and the radar-inferred core of the supercell that produced hail during this case.

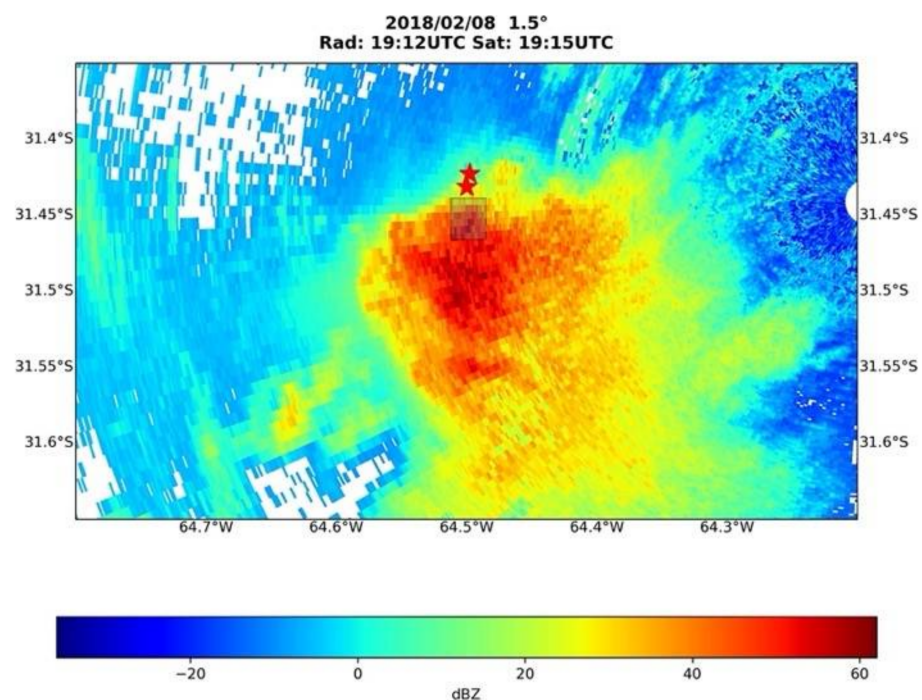


Figure 13. Reflectivity images from RMA1 radar showing the northern convective system (supercell) on 8 February 2018 and locations (red stars) where hail fall was reported at 19:20 UTC in Calle San Lorenzo and Calle Tupungato. The grey box is the satellite-tracked core, which was associated with the supercell producing the hail marked by the red stars with an area of high reflectivity. This radar reflectivity image was from an elevation angle of 1.5 deg.

3.2.3. Temporal Trends in Satellite Data

Similar to the 14 December case, the temporal evolution of the northern cell's convective core (highlighted by the black box in Figure 12) was quantified using satellite data leading up to, during, and after the reported hail. As seen in Figure 14a, brightness temperatures showed a gradual decrease from 224 down to 205 K from 17:30 to 18:30 UTC with a cooling rate of -18 K/h, already reaching colder temperatures than the tropopause (215 K). After this initial decrease, brightness temperatures remained within an average of 203 K, with a standard deviation of 3 K between 18:30 and 20:45 UTC, times in which hail was collected. Similar to the 14 December case, this trend can be linked back to satellite-based evolution displayed in Figure 12; the cell initially strengthened rapidly then remained relatively steady, while another nearby cell appeared in the proximity of the convective core at 19:00 UTC that was not associated with confirmed hail reports. During this period (18:30 to 20:45 UTC), the tri-spectral analysis showed positive values staying within an average of 2 K (Figure 14c), indicating the dominance of ice crystals. During the same time, ice crystal size analysis was within an average of 5 K (Figure 14d), indicating that

small crystals prevailed in the cloud through the hail events on 8 February, similar to the 14 December case.

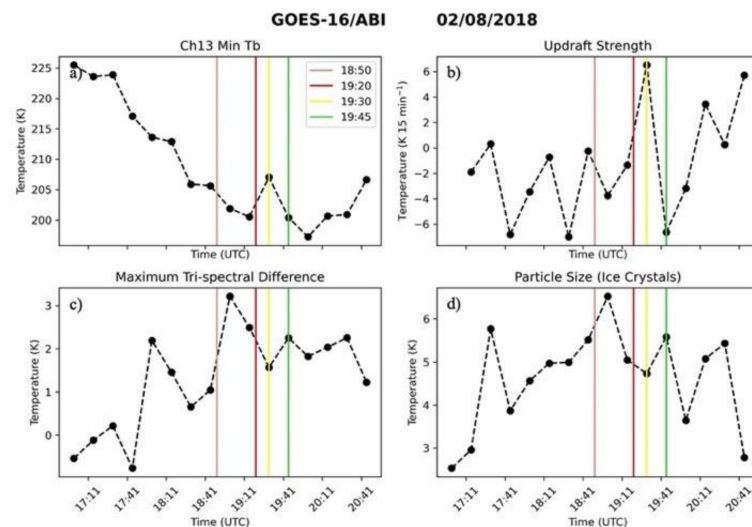


Figure 14. Temporal variation for 8 February 2018 of (a) local minimum $10.35\ \mu\text{m}$ Tb (K) as a proxy for storm strength; (b) temporal trend of $10.35\ \mu\text{m}$ Tb (K min¹⁵) to identify cooling and warming episodes related to updraft weakening and strengthening, respectively; (c) maximum tri-spectral difference (K), which indicates the mass of ice crystals through full depth of cloud (positive values, presence of ice crystals; negative values, presence of water droplets); and (d) maximum difference between 8.5- and $11.2\text{-}\mu\text{m}$ Tb (K), which provides the predominant ice crystal size in the cloud (greater positive values, smaller ice crystals; smaller positive values, larger ice crystals). Light coral, red, yellow, and lime green lines mark the time of hail fall. Data used in this analysis correspond to 15 min intervals starting from 17:00 UTC.

Regarding the updraft strength, the change in brightness temperatures prior to each hail report revealed negative values (i.e., slight strengthening) for the first three reports (-0.3 , -1 , -1 K/15 min, respectively) associated with a hail size of 5 cm at 18:50 UTC, 8/17 cm at 19:20, and 4 cm at 19:30 UTC and positive values in the last hail report (7 K/15 min). Although data showed that for the first three hail times the updraft slightly strengthened before each one, and the relative magnitude of that increase decreased with time, suggesting systematic weakening of the updraft leading up to the largest hail report at 19:20 UTC. Therefore, as in the 14 December case, the hail reports occurred during a mature phase of the storm while the system was undergoing a slight weakening. Similarly, there was also a strong presence of small ice crystals through all hail reports including a steady increase in the concentration of small ice crystals leading up to the hail reports (Figure 14d).

3.3. 24 October 2020 Supercell

3.3.1. Environmental Setting

The 24 October case exhibited similar behavior as the northern cell observed during the 8 February case. Around 15:20 UTC, convection initiated east of the Sierras Grandes (Figure 1; yellow circle), followed by rapid growth. This intense convective cell resulted in four confirmed hail reports (18:20, 18:32, 18:35, and 19:20 UTC, in Villa Carlos Paz, San Antonio de Redondo, and Villa Allende, respectively; Table 1) after which by 19:50 UTC, it started to dissipate. Figure 15 shows isobaric charts at 500 and 850 hPa at 00:00 and 12:00 UTC. Similar to 14 December, a mid-level trough at 500 hPa was observed but different to 14 December, it did not show any movement between earlier and later in the day on 24 October. At the same height, a low-pressure system was positioned west of the Patagonia region, while on 14 December, it was located south over the Patagonia region. Additionally, a lower amplitude low-level trough (compared to 14 December) west of the

Andes was present, progressing lee-side of the Andes at the 850 mb level. Similar to the 14 December case and different to the February case, there was a large area of anomalously high humidity that extended through central Argentina (Figure 16), potentially suggesting the presence of the SALLJ ushering in moisture from the north. Only one sounding at 12:00 UTC was available at Córdoba Airport during this event (Figure 17), and it showed a low-level jet (25 kt winds around 850 hPa in the sounding) that likely contributed to the moisture in low levels. A capping inversion was also observed, produced by subsiding cold, dry air from the Andes. Mixed-layer CAPE values for this case were ~ 932 J/kg, which were lower than the 14 December case (2300 J/kg) and higher than the 8 February case (considering that the 8 February case sounding was not representative, and only the model runs showed enough elevated CAPE for that event).

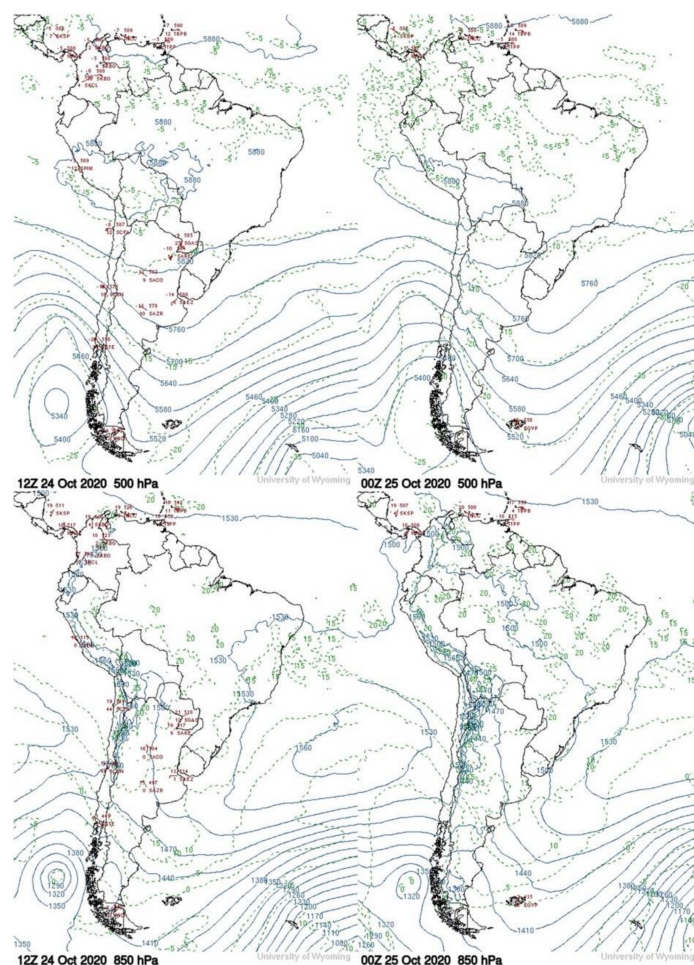


Figure 15. Isobaric chart at 500 and 850 hPa for 12:00 UTC on 24 October 2020 and 00:00 UTC on 25 October 2020 from the University of Wyoming [40]. Solid blue lines show isobars; dashed green lines show the isotherms; and red text are surface station observations.

With similarly limited elevated CAPE east of the SDCs, convection in this case evolved similarly to 8 February with initiation solely over the higher elevations in the late afternoon. Compared to 14 December, the sounding analysis for this October case indicated a weaker low-level jet and 500-hPa wind speeds that, in addition to the lower CAPE values, indicated less favorable conditions for convection and/or severe weather. Nonetheless, this case showed similar convective evolution patterns seen in the northern cell on 8 February (i.e., similar geographical region, similar convection initiation times). SMN forecasters discussed on 23 October that conditions were favorable for strong rains, isolated storms with varying intensities, cloudburst of intense rain, lightning activity, and hail fall extending through 24 October in regions similar to the 8 February case where hail was reported.

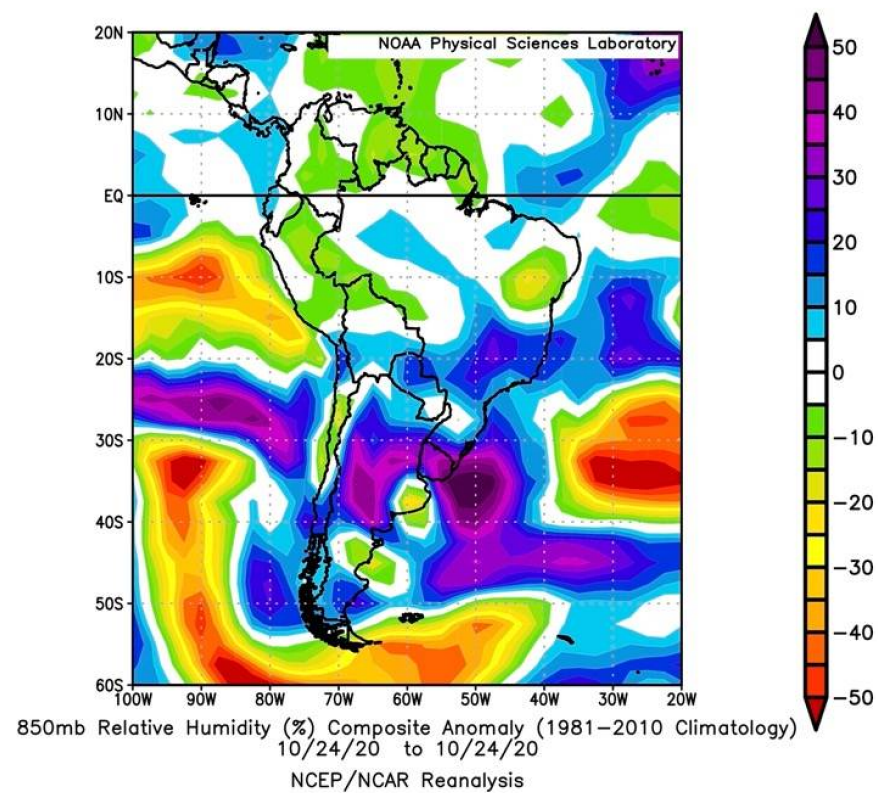


Figure 16. Relative humidity composite anomaly at 850 mb for 24 October 2020 [42].

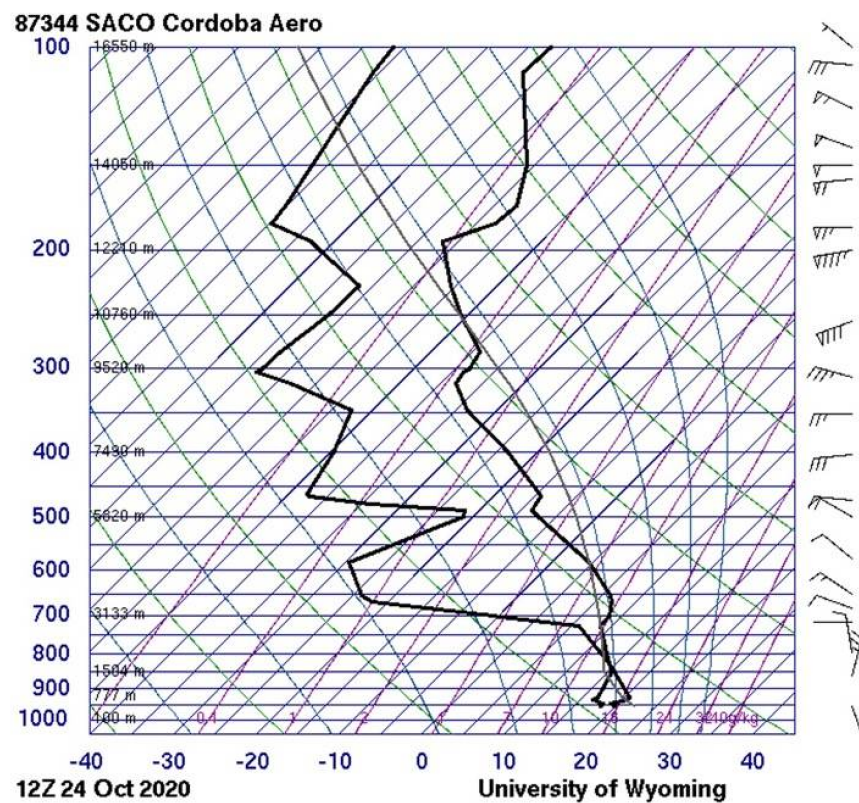


Figure 17. Atmospheric soundings from Córdoba Airport in Córdoba Province, Argentina at 1200 UTC on 24 October 2020 [41].

3.3.2. Convective Characteristics

Channel 11 brightness temperatures from this case (Figure 18) showed convective cells developing east of the Sierras Grandes, which could indicate that there was some orographic lifting that aided in the rapid growth of this smaller storm, similar to the 8 February case. The white box includes the area over which the convective core was tracked before, during, and after the reported hail fall until it dissipated. Even though this cell had a shorter lifetime than the northern cell on 8 February and exhibited warmer brightness temperatures, it did produce four hail events at 18:20, 18:32, 18:35, and 19:27 UTC (Figure 1c). Figure 18 shows a gradual decrease in the brightness temperatures through time. These were similar temperatures to the southern cell in the 8 February case, which could lead to the assumption that the southern cell might have had hail events, or at least graupel, which were not recorded because of the lack of observers in the area. After the hail falls, the October tracked cell started to show warmer temperatures until it dissipated. Compared to 8 February and 14 December, this system also had a shorter life span.

These satellite plots also showed clear AACP and enhanced V signatures in this storm through the first three hail reports, suggestive of severe weather. For the last hail report, there was no AACP and enhanced V signature apparent in the satellite images.

Radar-based analysis, as seen in Figure 19, showed that the convective cell responsible for the four hail events in different locations in Villa Carlos Paz, San Antonio de Redondo, and Villa Allende (stars in Figure 19 only show San Antonio de Redondo and VCP N, which were the nearest times for hail fall to the radar image time) was a supercell (as also confirmed by radar velocity data during this time, not shown). A weak hook echo at 18:27 UTC was observed similarly to the 8 February case. An overlay of convective core pixels from Channel 11 (gray box) over this radar reflectivity image aligned closely, which shows that the convective core in both radar and satellite images were associated with hail reports in the region.

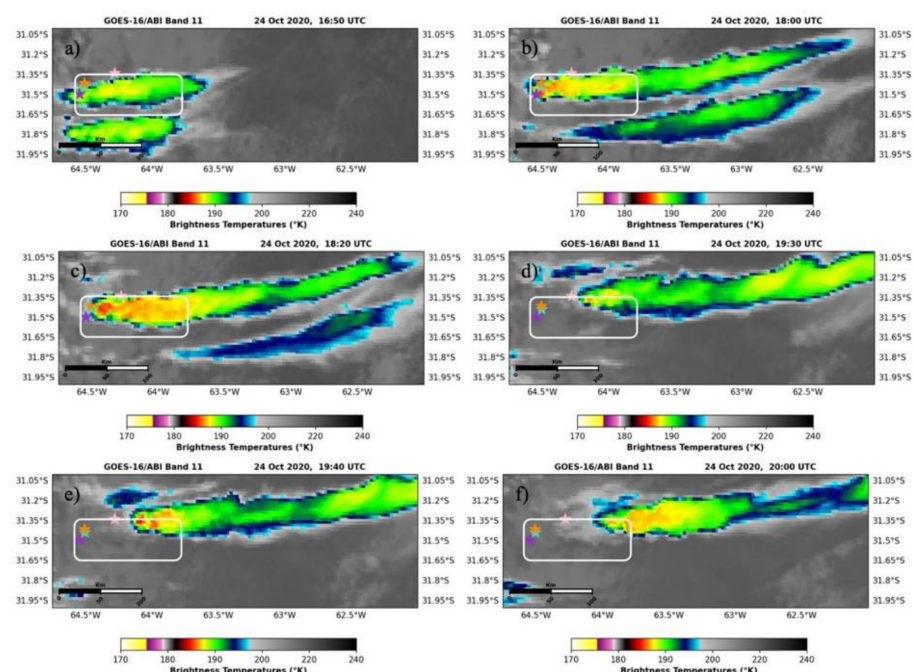


Figure 18. Subfigures (a–f) are figures in one-hour intervals from GOES-16, Channel 11, showing the convective system (supercell) studied on 24 October 2020. White box highlights the convective core analysis bounds. As shown in Table 1, these images were just before and during the recorded hailstorms. Each star is associated with each hail report: 18:20 UTC (turquoise), 18:32 UTC (dark orchid), 18:35 UTC (dark orange), 19:27 UTC (light pink) at VCP, San Antonio de Redondo, VCP North and Villa Allende, respectively.

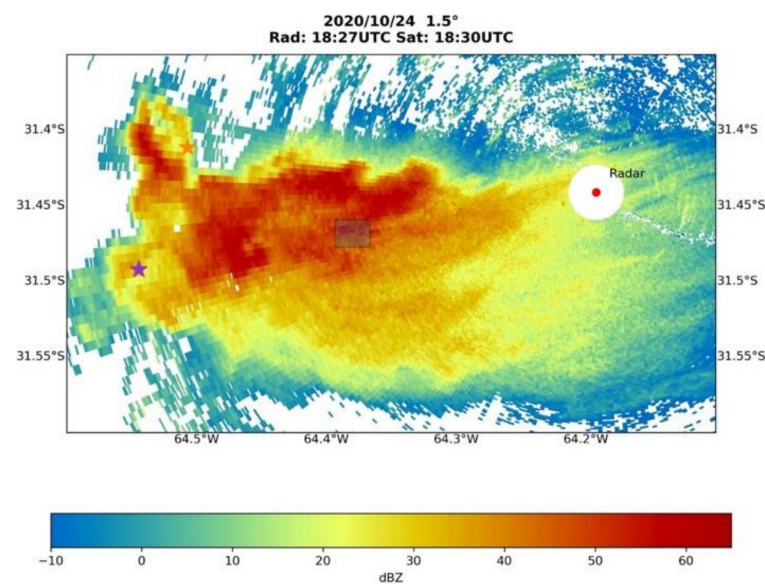


Figure 19. Reflectivity image from the RMA1 radar showing the supercell that developed on 24 October 2020 and locations (purple and orange stars) where hail fall was reported at 19:32 and 19:35 UTC, respectively. The grey box is the satellite-tracked core, which was associated with the supercell producing the hail marked by the dark orange and dark orchid stars with an area of high reflectivity. This radar reflectivity image was from an elevation angle of 1.5 deg.

3.3.3. Temporal Trends in Satellite Data

Following the same satellite-based analysis as for the previous hail cases, the evolution of the convective core was analyzed for this system with respect to the timing of the hail reports. Figure 20a shows that the brightness temperatures decreased from 223 K to 216 K from 17:00 through to 18:00 UTC, a cooling rate of -7 K/h, already reaching colder temperatures than the tropopause (228 K). After this initial decrease, brightness temperatures remained within an average of 218 K, with a standard deviation of 4 K between 18:00 and 20:00 UTC (Figure 20b), times in which hail was collected. This pattern was also observed in the 14 December and 8 February cases. During this period (18:00 to 20:00 UTC), the tri-spectral analysis showed positive values, staying within an average of -0.4 K (Figure 20c), indicating the presence of water droplets. During the same time period, the ice crystal size analysis was within an average of 1 K (Figure 20d), indicating a predominant presence of larger ice crystals in the cloud through the first three hail events. In the case of the fourth hail report, a negative value was present prior to the hail (Figure 20d), interpreted as fewer ice crystals present in the cloud (Ackerman et al. 1990), which differed from observations in previous cases.

Regarding the updraft, positive values of brightness temperature differences (Figure 20b) were observed prior to all reports (1, 0.2, 0.2, 3 K/10 min, respectively) associated with hail sizes of 3 cm at 18:20 UTC and 1.3 cm at 19:32/18:35/19:27 UTC. Generally, the updraft strength, similar to the 14 December case, weakened for all reports. The presence of water droplets was noted for all reports (Figure 20c) with average values of -0.4 K, different to both 14 December and 8 February (3 and 2 K, respectively). Finally, larger ice crystals were observed in the 24 October case (low positive values; Figure 20d) compared to the 14 December and 8 February cases (5 K; i.e., higher positive values), which can be attributed to the fact that this system showed warmer cloud top brightness temperatures compared to the 14 December and 8 February cases.

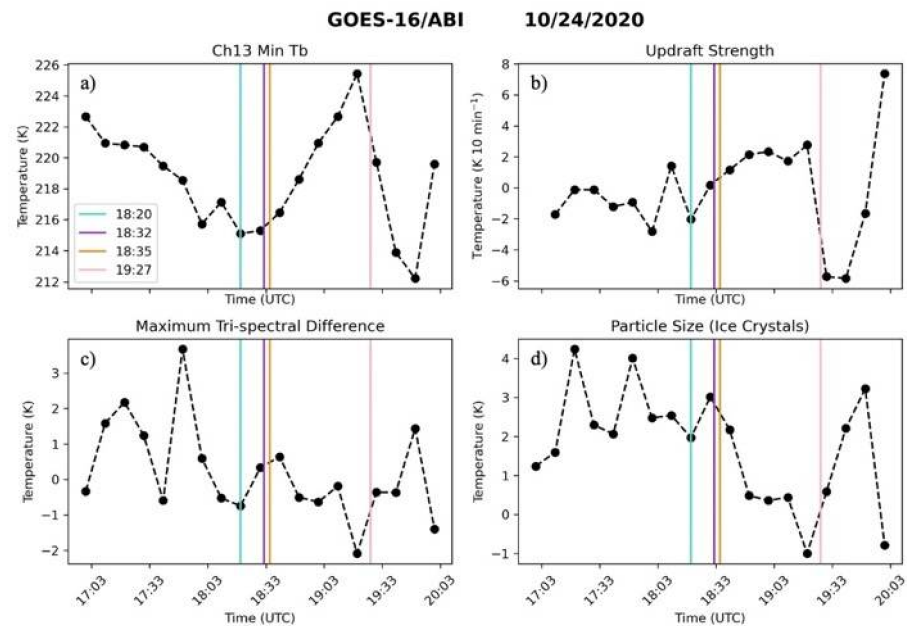


Figure 20. Temporal variation for 24 October 2020 of (a) local minimum $10.35\ \mu\text{m}$ Tb (K) as a proxy for storm strength; (b) temporal trend of $10.35\ \mu\text{m}$ Tb (K min 15) to identify cooling and warming episodes related to updraft weakening and strengthening, respectively; (c) maximum tri-spectral difference (K), which indicates the mass of ice crystals through full depth of cloud (positive values, presence of ice crystals; negative values, presence of water droplets); and (d) maximum difference between 8.5 and $11.2\ \mu\text{m}$ Tb (K), which provides the predominant ice crystal size in the cloud (greater positive values, smaller ice crystals; smaller positive values, larger ice crystals). Turquoise, dark orchid, dark orange, and light pink lines mark the time of hail fall. Data used in this analysis correspond to 10 min intervals starting from 17:00 UTC.

4. Discussion

This study aimed to evaluate how well temporal trends in geostationary satellite signatures could be used to infer hail in Argentina through verified hail reports from three storm cases exhibiting different storm modes in different large-scale environments. Previous studies using hail proxies (e.g., [15]), model output (e.g., [23]), or limited radar datasets (e.g., [19]) noted that deep convective systems in this region of the world were most often associated with increased moisture from the SALLJ, dry air subsidence east of the Andes capping that low-level moist layer, and lee cyclogenesis resulting from the passage of an upper-level trough. Specific to hail-producing storms, Bruick et al. (2019) [15] noted anomalously warm and moist low levels likely corresponded to the strong LLJ corresponding to satellite-based proxies of hail. The hail-producing MCS analyzed in this study (14 December case) exhibited all these favorable environmental parameters and provided the much-needed verification of hail occurring overnight from a MCS formed in this strongly forced environment. While there were upper-level troughs present leading up to the supercell cases, these were either located much farther south of the Córdoba domain (8 February) or remained stationary west of the Andes with a much lower amplitude (24 October).

During both supercell cases, the Córdoba soundings showed relatively limited instability, suggesting that it was not representative of the more locally favorable environment over the mountains where these convective cells initially formed during the afternoon (e.g., [33]). Therefore, in summary, the hail cases in this study included a strongly forced MCS, consistent with the previous literature of environments supporting multicellular systems producing hail overnight in this region (14 December), while more local forcing (e.g., upslope flow) was inferred for the supercell cases (8 February and 24 October) to access elevated instability during the afternoon. The only case with hail mentioned in

the official SMN forecast was 24 October, while the forecasts for the other storms focused more on other impacts such as heavy rainfall, highlighting the need to further study the environments of hail-producing storms of varying organization modes in this region. Hail produced from nocturnal MCSs (e.g., [15]) particularly requires further study, as supercells have generally been more widely studied in the context of hail in SESA and in the U.S.

To potentially aid in the nowcasting of these hail-producing storms, geostationary satellite data were used to describe the temporal and spatial evolution of these storms relative to the time and location of hail reports. Both the 8 February 2018 and 24 October 2020 supercell cases were more localized storms initiating over the high terrain during the afternoon, producing hail (including 17 cm hail on 8 February, [33,34]) in the evening within 3 and 3.5 h of initiation, respectively, whereas the 14 December MCS formed over the San Luis plains later in the evening, growing upscale and strengthening after dark, producing hail overnight within 5 h of initiation. These systems intensified over the mountains with similarly low brightness temperatures on 8 February and 13 December, despite larger hail falling on 8 February, and with warmer brightness temperatures observed on 24 October. Additionally noted was a southern cell developing over the San Luis plains on 8 February with warmer brightness temperatures, comparable to 24 October. This convective system did not have hail reports, although it is difficult to say whether the system did produce hail because it happened in a remote area.

An evaluation of the temporal evolution of satellite-derived signatures leading up to and during the hail events was conducted for all cases. Unlike a similar analysis from Ribeiro et al. (2019) [25] for a hail-producing storm in Brazil, individual convective cores were identified and tracked instead of using their method of calculating brightness temperature thresholds as those thresholds would have varied considerably across our three cases. This core tracking followed an approach more similar to Borque et al. (2020)'s [32] analysis of a supercell in Argentina by identifying minimum brightness temperatures from Channel 13, calculating inflection points to isolate the convective core and track it through time. Through this method, multiple channels from GOES-16 were evaluated within the core to track the changes in minimum brightness temperatures from Channel 13 as a measure of updraft intensity (e.g., [31,37]) and to infer the presence and concentrations of varying sizes of ice crystals [38] leading up to the verified hail reports.

In combination with each other, this satellite analysis enabled the identification of signatures and temporal patterns to link verified hail to a satellite-tracked convective core for prospectively improving short-term hail forecasting. All storms initially deepened with cooling rates of -19 K/h, -18 K/h, and -4 K/h for 14 December, 8 February, and 24 October, respectively, reaching minimum brightness temperatures (198 K, 14 December; 202 K, 8 February; 218 K, 24 October) that were equal to or lower than the temperatures at the tropopause (198, 215, and 228 K, respectively). Not surprisingly, then, AACPs and enhanced V signatures were observed in all cases prior to a hail report (e.g., at 31.46° S, 64.47° W at 18:00 UTC and 31.42° S, 64.38° W at 18:20 UTC), further validating the association of these signatures as indicators for severe weather (e.g., [49]). After reaching these minimum brightness temperatures, the temporal trend oscillated around values close to the tropopause temperature, varying no more than 3–4 K between satellite times (15 min for 8 February and 14 December; 10 min for 24 October), indicating the overall maintenance of an updraft within these mature systems during the times of the hail fall. Within these more subtle variations emerged a trend where there was a slight weakening of the updraft just prior to each hail report, a trend that differed from that observed in the Ribeiro et al. (2019) [25] analysis.

For both the 14 December and 8 February cases, analysis to infer ice crystals in the cloud noted increasing concentrations of small ice crystals leading up to the hail, particularly the larger hail reports. The 24 October case differed in that negative values (with an average of -0.4 K) were observed in the tri-spectral analysis, which indicates water droplets as well as a weaker or nonexistent signature of small crystals in the cloud associated with smaller hail in this case. This difference is consistent with the lower

brightness temperature values compared to the 14 December and 8 February cases as the 24 October cell did not achieve as much vertical development as that seen in the other two cases. Therefore, this analysis suggests that satellite signatures highlighting the dominant presence of small ice crystals within an intense, mature convective storm could point to the possibility of hail for different storm modes. Differences in the observed trends, here compared to those described in Ribeiro et al. (2019) [25], could be related to (1) the method of identifying the convection for the satellite-based temporal analysis; (2) that tracking cores within MCSs may present more of a challenge through more variations in signatures as cores intensify and weaken throughout time; or (3) that using smoothed mesoscale domain data to a 5-min resolution provided more robust signatures compared to the 10- and 15-min trends.

5. Conclusions

The promising results from this comparison between three hail-producing cases provided the motivation to look further at the different types of environments that favor hail-producing storms in this region. This continued effort is necessary to better understand hail formation and forecasting specifically in this region, given that these hail-producing systems formed under different environmental conditions, times of day, and locations relative to the mountains as well as included both supercells and MCSs. Through a comparison of different satellite-based trends relative to our verified hail reports, our analysis not only noted signatures associated with the hail that could be further explored for nowcasting efforts, but also suggests that a cell with no verified hail due to the remoteness of the area (e.g., the southern cell on the 8 February case likely produced hail as it showed similar satellite trend patterns to the tracked cells with hail reports). This motivates the need to find verified null cases in this region (i.e., convective systems confirmed not to have produced hail) to further confirm the signatures described in this study. Therefore, collaborations with the citizen science program “Cosecheros de Granizo” will continue to find these null cases and strengthen this project’s analysis. The goal will be to use these key signatures to discriminate between hail producing and non-hail producing convective systems, given verified hail at the surface, to start improving hail nowcasting in this region.

This goal also motivates the need to include additional satellite-based signatures in this analysis using other satellite products. More specifically, geostationary lightning data could be used to investigate signatures related to the lightning jump and hail production (as in [25] and other studies), but unfortunately, this dataset was not available for all cases analyzed in this study. Another possible route would be to focus on mesoscale sectors such as Ribeiro et al. (2019) [25], as they stated that their strongest signatures were at the 5-min scale, and not at 10 or 15 min. Regardless of the number of products used, future work must include a variety of convective modes, as demonstrated in this study, as this region exhibits a strong nocturnal peak in hail from MCSs, thus expanding our inferences beyond supercells that tend to be the focus of this type of analysis. This analysis could also expand the cases to the U.S. using confirmed hail reports to explore similar satellite trends that would strengthen the analysis used in this project.

In general, future goals will be to put this analysis back in the context of hail formation in general given different environmental conditions, especially because of the differences in satellite-based signatures for different hail sizes and storm modes. Previous research showed how aerosols may influence the temperature at which ice nucleation can happen in the cloud [50], especially when there is large-scale forcing where the air source comes from different locations versus a more localized source [49,51]. Having the actual hail samples will aid in understanding this potential influence in understanding and predicting hail formation and size. The goal is to improve hail forecasting through improved understanding of the processes and ingredients in this region and how remote sensing can aid in the nowcasting aspect of determining which cells may produce hail based on that improved understanding.

Author Contributions: Conceptualization, A.C.B.A. and L.E.A.; methodology, A.C.B.A., A.K.R. and L.E.A.; software, A.C.B.A.; validation, A.K.R. and L.E.A.; formal analysis, A.C.B.A., A.K.R. and L.E.A.; investigation, A.C.B.A., A.K.R. and L.E.A.; resources, A.K.R. and L.E.A.; data curation, L.E.A.; writing—original draft preparation, A.C.B.A.; writing—review and editing, A.C.B.A., A.K.R., L.E.A. and A.R.D.; visualization, A.C.B.A.; supervision, A.K.R., L.E.A. and A.R.D.; funding acquisition, A.K.R., L.E.A. and A.R.D. All authors have read and agreed to the published version of the manuscript.

Funding: This research was funded by the University of Wisconsin Advanced Opportunity Fellowship and National Science Foundation (grant no. AGS-1640452, AGS-1661768 and AGS-2146708).

Data Availability Statement: Hail data for this research project were collected through the Cosecheros de Granizo program with the patronage of the Ministry of Science and Technology of Cordoba Province for samples in 2018 and the Hydrometeorological Observatory of Cordoba for samples collected from 2020 onward. Satellite data, isobaric charts, soundings, and humidity composites are publicly available. Radar data from RMA1 are available upon request to the Argentinian government.

Acknowledgments: We would like to acknowledge the Secretary of Science and Technology of the National University of Cordoba for research grants, the Cordoba Radar Group for providing the radar data and the advice in using these data, and Pete Pokrandt, system programmer for the UW-Madison AOS Department, for his help in the early stages of this project's satellite data processing and advice later on.

Conflicts of Interest: The authors declare no conflict of interest.

References

1. Kumjian, M.R.; Lebo, Z.J.; Ward, A.M. Storms Producing Large Accumulations of Small Hail. *J. Appl. Meteorol. Climatol.* **2019**, *58*, 341–363. [\[CrossRef\]](#)
2. Allen, J.T.; Tippet, M.K.; Kaheil, Y.; Sobel, A.H.; Lepore, C.; Nong, S.; Muehlbauer, A. An Extreme Value Model for U.S. Hail Size. *Mon. Weather Rev.* **2017**, *145*, 4501–4519. [\[CrossRef\]](#)
3. Sander, J.; Eichner, J.F.; Faust, E.; Steuer, M. Rising Variability in Thunderstorm-Related U.S. Losses as a Reflection of Changes in Large-Scale Thunderstorm Forcing. *Weather Clim. Soc.* **2013**, *5*, 317–331. [\[CrossRef\]](#)
4. Changnon, S.A. Temporal and Spatial Distributions of Damaging Hail in the Continental United States. *Phys. Geogr.* **2008**, *29*, 341–350. [\[CrossRef\]](#)
5. Zipser, E.J.; Nesbitt, S.W.; Liu, C.; Yorty, D.P. Where Are the Most Intense Thunderstorms on Earth? *Bull. Am. Meteorol. Soc.* **2006**, *1057*–1071. [\[CrossRef\]](#)
6. Rasmussen, K.L.; Zuluaga, M.D.; Houze, R.A., Jr. Severe Convection and Lightning in Subtropical South America. *Geophys. Res. Lett.* **2014**, *41*, 7359–7366. [\[CrossRef\]](#)
7. Cecil, D.J.; Blankenship, C.B. Toward a Global Climatology of Severe Hailstorms as Estimated by Satellite Passive Microwave Imagers. *J. Clim.* **2012**, *25*, 687–703. [\[CrossRef\]](#)
8. Johnson, A.W.; Sugden, K.E. Evaluation of Sounding-Derived Thermodynamic and Wind-Related Parameters Associated with Large Hail Events. *Electron. J. Severe Storms Meteor.* **2014**, *9*, 1–42.
9. Jewell, R.; Brimelow, J. Evaluation of Alberta Hail Growth Model Using Severe Hail Proximity Soundings from the United States. *Weather Forecast* **2009**, *24*, 1592–1608. [\[CrossRef\]](#)
10. Edwards, R.; Thomson, R.L. Nationwide Comparisons of Hail Size with WSR-88D Vertically Integrated Liquid Water and Derived Thermodynamic Sounding Data. *Weather Forecast* **1998**, *13*, 277–285. [\[CrossRef\]](#)
11. Allen, J.T.; Giammanco, I.M.; Kumjian, M.R.; Jurgen Punge, H.; Zhang, Q.; Groenemeijer, P.; Kunz, M.; Ortega, K. Understanding Hail in the Earth System. *Rev. Geophys.* **2020**, *58*, e2019RG000665. [\[CrossRef\]](#)
12. Il, D.J.G.; Haupt, S.E.; Nychka, D.W.; Thompson, G. Interpretable Deep Learning for Spatial Analysis of Severe Hailstorms. *Mon. Weather Rev.* **2019**, *147*, 2827–2845. [\[CrossRef\]](#)
13. Smith, B.T.; Thompson, R.L.; Grams, J.S.; Broyles, C.; Brooks, H.E. Convective Modes for Significant Severe Thunderstorms in the Contiguous United States. Part I: Storm Classification and Climatology. *Weather Forecast* **2012**, *27*, 1114–1135. [\[CrossRef\]](#)
14. Bang, S.D.; Cecil, D.J. Constructing a Multifrequency Passive Microwave Hail Retrieval and Climatology in the GPM Domain. *J. Appl. Meteorol. Climatol.* **2019**, *58*, 1889–1904. [\[CrossRef\]](#)
15. Bruck, Z.S.; Rassumen, K.L.; Cecil, D.J. Subtropical South American Hailstorm Characteristics and Environments. *Mon. Weather Rev.* **2019**, *147*, 4289–4304. [\[CrossRef\]](#)
16. Ni, X.; Liu, C.; Cecil, D.J.; Zhang, Q. On the Detection of Hail Using Satellite Passive Microwave Radiometers and Precipitation Radar. *J. Appl. Meteorol. Climatol.* **2017**, *56*, 2693–2709. [\[CrossRef\]](#)
17. Nesbitt, S.W.; Salio, P.V.; Ávila, E.; Bitzer, P.; Carey, L.; Chandrasekar, V.; Deierling, W.; Dominguez, F.; Dillon, M.E.; Garcia, C.M.; et al. A Storm Safari in Subtropical South America: Proyecto RELAMPAGO. *Bull. Am. Meteorol. Soc.* **2021**, *102*, E1621–E1644. [\[CrossRef\]](#)

18. Arena, L.; Crespo, A. *Recopilación de Estudios Primarios de Caracterización Cristalográfica de Granizos y de las Tormentas que los Originan*; Universidad Nacional de Córdoba: Córdoba, Argentina, 2019.
19. Mulholland, J.P.; Nesbitt, S.W.; Trapp, R.J.; Rasmussen, K.L.; Salio, P.V. Convective Storm Life Cycle and Environments near the Sierras de Córdoba, Argentina. *Mon. Weather Rev.* **2018**, *146*, 2541–2557. [\[CrossRef\]](#)
20. Vidal, L. Convección Extrema Sobre Sudamérica: Estructura Interna, Ciclos de Vida e Influencia de la Topografía en la Iniciación. Ph.D. Thesis, Universidad de Buenos Aires, Buenos Aires, Argentina, 2014.
21. Sasaki, C.R.S.; Rowe, A.K.; McMurdie, L.A.; Rasmussen, K.L. New Insights into the South American Low-Level Jet from RELAMPAGO Observations. *Mon. Weather Rev.* **2022**, *150*, 161. [\[CrossRef\]](#)
22. Jones, C. Recent Changes in the South America Low-Level Jet. *Npj Clim. Atmos. Sci.* **2019**, *2*, 20. [\[CrossRef\]](#)
23. Rasmussen, K.L.; Houze, R.A., Jr. Convective Initiation near the Andes in Subtropical South America. *Mon. Weather Rev.* **2016**, *144*, 2351–2374. [\[CrossRef\]](#)
24. Salio, P.; Nicolini, M.; Saulo, A.C. Chaco Low-Level Jet Events Characterization during the Austral Summer Season. *J. Geophys. Res. Atmos.* **2002**, *107*, ACL 32-1–ACL 32-17. [\[CrossRef\]](#)
25. Ribeiro, B.Z.; Machado, L.A.T.; Huamán Ch, J.H.; Biscaro, T.S.; Reitas, E.D.; Mozer, K.W.; Goodman, S.J. An Evaluation of the GOES-16 Rapid Scan for Nowcasting in Southeastern Brazil: Analysis of a Severe Hailstorm Case. *Weather Forecast* **2019**, *34*, 1829–1847. [\[CrossRef\]](#)
26. Merino, A.; López, L.; Sánchez, J.L.; García-Ortega, E.; Cattani, E.; Levizzani, V. Daytime Identification of Summer Hailstorm Cells from MSG Data. *Nat. Hazards Earth Syst. Sci.* **2014**, *14*, 1017–1033. [\[CrossRef\]](#)
27. Ravinder, A.; Reddy, P.K.; Prasad, N. *Detection of Wavelengths for Hail Identification Using Satellite Imagery of Clouds*; IEEE: Madrid, Spain, 2013; pp. 205–211.
28. Bauer-Messmer, B.; Waldovel, A. Satellite Data Based Detection and Prediction of Hail. *Atmos. Res.* **1997**, *43*, 217–231. [\[CrossRef\]](#)
29. Konduru, R.T.; Kishtawal, C.M.; Shah, S. A New Perspective on the Infrared Brightness Temperature Distribution of the Deep Convective Clouds. *J. Earth Syst. Sci.* **2013**, *122*, 1195–1206. [\[CrossRef\]](#)
30. Roca, R.; Ramanathan, V. Scale Dependence of Monsoonal Convective Systems over the Indian Ocean. *J. Clim.* **2000**, *13*, 1286–1298. [\[CrossRef\]](#)
31. Müller, R.; Jerg, M.; Haussler, S.; Heizenreder, D. A Novel Approach for the Detection of Developing Thunderstorm Cells. *Remote Sens.* **2019**, *11*, 443. [\[CrossRef\]](#)
32. Borque, P.; Vidal, L.; Rugna, M.; Lang, T.J.; Nicora, M.G.; Nesbitt, S.W. Distinctive Signals in 1-Min Observations of Overshooting Tops and Lightning Activity in a Severe Supercell Thunderstorm. *J. Geophys. Res. Atmos.* **2020**, *125*, e2020JD032856. [\[CrossRef\]](#)
33. Kumjian, M.R.; Gutierrez, R.; Soderholm, J.S.; Nesbitt, S.W.; Maldonado, P.; Luna, L.M.; Marquis, J.; Bowley, K.A.; Imaz, M.A.; Salio, P. Gargantuan Hail in Argentina. *Bull. Am. Meteorol. Soc.* **2020**, *101*, E1241–E1258. [\[CrossRef\]](#)
34. Arena, L.E. *Granizos Gigantes de Córdoba-Argentina I. El Coloso Victoria*; Universidad Nacional de Córdoba (UNC): Córdoba, Argentina, 2020.
35. Mecikalski, J.R.; Bedka, K.M. Forecasting Convective Initiation by Monitoring the Evolution of Moving Cumulus in Daytime GOES Imagery. *Mon. Weather Rev.* **2006**, *134*, 49–78. [\[CrossRef\]](#)
36. Roberts, R.D.; Rutledge, S. Nowcasting Storm Initiation and Growth Using GOES-8 and WSR-88D Data. *Weather Forecast* **2003**, *18*, 562–584. [\[CrossRef\]](#)
37. Adler, R.F.; Fenn, D.D. Thunderstorm Vertical Velocities Estimated from Satellite Data. *J. Atmos. Sci.* **1979**, *36*, 1747–1754. [\[CrossRef\]](#)
38. Ackerman, S.A.; Smith, W.L.; Revercomb, H.E.; Spinhirne, J.D. The 27–28 October 1986 FIRE IFO Cirrus Case Study: Spectral Properties of Cirrus Clouds in the 8–12 μ m Window. *Mon. Weather Rev.* **1990**, *118*, 2377–2388. [\[CrossRef\]](#)
39. Strabala, K.I.; Ackerman, S.A.; Menzel, W.P. Cloud Properties Inferred from 8–12-Mm Data. *J. Appl. Meteorol. Climatol.* **1994**, *33*, 212–229. [\[CrossRef\]](#)
40. University of Wyoming. Upper Air Weather Maps. Available online: <https://weather.uwyo.edu/upperair/uamap.shtml> (accessed on 26 March 2022).
41. University of Wyoming. Atmospheric Soundings. Available online: <https://weather.uwyo.edu/upperair/sounding.html> (accessed on 26 March 2022).
42. NOAA Physical Sciences Laboratory. Daily Climate Composites. Available online: <https://psl.noaa.gov/data/composites/day/> (accessed on 26 March 2022).
43. NCAR Earth Observing Laboratory. RELAMPAGO Field Catalog. Available online: <https://catalog.eol.ucar.edu/relampago> (accessed on 26 March 2022).
44. Piersante, J.; Schumacher, R.; Rasmussen, K. Comparison of Biases in Warm-Season WRF Forecasts in North and South America. *Weather Forecast* **2021**, *36*, 979–1101. [\[CrossRef\]](#)
45. Montini, T.L.; Jones, C.; Carvalho, L.M.V. The South American Low-Level Jet: A New Climatology, Variability, and Changes. *J. Geophys. Res. Atmos.* **2019**, *124*, 1200–1218. [\[CrossRef\]](#)
46. Vera, C.; Baez, J.; Douglas, M.; Emmanuel, C.B.; Marengo, J.; Meitin, J.; Nicolini, M.; Nogues-Paegle, J.; Paegle, J.; Penalba, O.; et al. The South American Low-Level Jet Experiment. *Bull. Am. Meteorol. Soc.* **2006**, *87*, 63–78. [\[CrossRef\]](#)
47. Saulo, A.C.; Nicolini, M. *The Atmospheric Conditions Preceding the Occurrence of a Strong Low Level Jets East of the Andes during January 1998*; Diego Portales Convention Center Santiago: Santiago, Chile, 1999.

48. Datos Argentina. Available online: <https://datos.gob.ar/> (accessed on 26 March 2022).
49. Bedka, K.; Murillo, E.M.; Homeyer, C.R.; Scarino, B.; Mersiovsky, H. The Above-Anvil Cirrus Plume: An Important Severe Weather Indicator in Visible and Infrared Satellite Imagery. *Weather Forecast* **2018**, *33*, 1159–1181. [[CrossRef](#)]
50. Michaud, A.B.; Dore, J.E.; Leslie, D.; Lyons, W.B.; Sands, D.C.; Priscu, J.C. Biological Ice Nucleation Initiates Hailstone Formation. *J. Geophys. Res. Atmos.* **2014**, *119*, 12186–12197. [[CrossRef](#)]
51. Beal, A.; Martins, L.D.; Martins, J.A.; Rudke, A.P.; de Almeida, D.S.; Costa, L.M.; Tarley, C.R.T. Evaluation of the Chemical Composition of Hailstones from Triple Border Paraná, Santa Catarina (Brazil) and Argentina. *Atmos. Pollut. Res.* **2021**, *12*, 184–192. [[CrossRef](#)]